scientific reports

Check for updates

OPEN

Design, synthesis, and multi-target evaluation of 4-phenyl quinoline-8-sulfonate thiosemicarbazones as potential anti-Alzheimer agents

Rahma Saeed[1], Hafiza Zara Tariq[2], Aiysha Althobaiti[3], Nastaran Sadeghian[4], Parham Taslimi[4], Mariya Al-Rashida[5], Talha Islam[5], Hamdy Khamees Thabet[6], Hina Aftab[1], Halil Şenol[7], Mubashir Ameen[8], Jing Li[2] & Zahid Shafiq[1]✉

Alzheimer's disease (AD) is a progressive neurodegenerative disorder marked by cognitive and memory decline. A novel series of 4-phenyl-quinoline-8-sulfonate-based thiosemicarbazones 5(a–r) were synthesized, characterized by some spectroscopic techniques and evaluated for their potential as anti-Alzheimer agents. Among them, compound 5c, bearing an *o*-fluoro phenyl group, showed multi-target inhibition with an IC_{50} values of 78.07 ± 3.14 µM acetylcholinesterase (AChE), 22.63 ± 2.81 µM butyrylcholinesterase (BChE) and 0.84 ± 0.01 µM monoamine oxidase A (MAO-A), showing higher inhibitory potential than the reference clorgyline with IC_{50} value 66.20 ± 4.01 µM. Other compounds, such as 5e, 5 g, 5b and 5q also exhibited significant inhibition across targets. Molecular docking confirmed strong binding interactions, particularly with the catalytic sites of AChE, BChE and MAO-A. These findings highlight 5c as a promising lead for multi-targeted AD therapy.

Keywords Thiosemicarbazones, Quinoline-8-sulfonate, Neurodegenerative disorders, Multi-target-directed ligands

Alzheimer's disease (AD) is a long-term neurological illness characterized by the steady deterioration of neurons, especially within the cholinergic system, and causing memory impairment, confusion, cognitive decline, and difficulty in reasoning and decision-making[1–3]. (AD) represents the principal etiology underlying dementia, contributing to approximately 50–75% of all diagnosed cases[4,5]. According to global health authorities, more than 55 million individuals worldwide are estimated to suffer from this chronic condition[6]. In (AD), several harmful changes take place in the brain. One of the main features is the formation of β-amyloid plaques, which are clumps of protein pieces called amyloid-β. These plaques build up between nerve cells and disturb their normal activity, causing damage to brain cells[7,8]. Another important problem is the presence of neurofibrillary tangles (NFTs) inside the nerve cells. These tangles are made from a protein called tau, which becomes faulty and gathers inside the cells, blocking the transport system and leading to cell death[9]. As the disease progresses, there is a gradual degeneration of nerve cells and their connections, especially in the hippocampus and cerebral cortex, which are important areas for memory and thinking[10]. A major part of this damage involves the cholinergic system, which uses a chemical messenger called acetylcholine (ACh) to help with memory and learning. In Alzheimer's patients, cholinergic neurons get damaged, and the levels of ACh drop[11]. Acetylcholinesterase (AChE) is an important enzyme that breaks down the neurotransmitter ACh, which helps with memory and learning. In (AD), the activity of AChE is frequently elevated in the regions surrounding amyloid plaques and neurofibrillary tangles, leading to a faster breakdown of acetylcholine and worsening memory loss[12]. Another related enzyme is butyrylcholinesterase (BChE). Although BChE plays a smaller role in a healthy brain, its activity increases in the later stages of Alzheimer's, when AChE levels decline. BChE becomes the primary enzyme

[1]Institute of Chemical Sciences, Bahauddin Zakariya University, Multan 60800, Pakistan. [2]School of Chemistry, Xi'an Jiaotong University, Xianning West Road, Xi'an 710049, China. [3]Department of Biochemistry, College of Medicine, Taif University, P.O. Box 11099, Taif 21944, Saudi Arabia. [4]Department of Biotechnology, Faculty of Science, Bartin University, 74110 Bartin, Turkey. [5]Department of Chemistry, Forman Christian College (A Chartered University), Lahore, Pakistan. [6]Center for Scientific Research and Entrepreneurship, Northern Border University, 73213 Arar, Saudi Arabia. [7]Department of Pharmaceutical Chemistry, Faculty of Pharmacy, Bezmialem Vakif University, 34093 Fatih, Istanbul, Turkey. [8]Faculty of Pharmacy, Bahauddin Zakariya University, Multan 60800, Pakistan. ✉email: zahidshafiq@bzu.edu.pk

breaking down ACh at this stage, contributing further to cognitive problems[13]. Monoamine oxidases (MAOs) break down neurotransmitters like dopamine and serotonin, producing harmful reactive oxygen species (ROS) as by-products. Increased MAO activity in (AD) leads to oxidative stress, and inhibiting these enzymes may help to protect nerve cells[14]. Due to the involvement of numerous targets in the (AD) network, multi-target-directed ligands (MTDLs) are considered a potential strategy for effective treatment[15]. By blocking MAOs, AChE and BChE, the levels of dopamine and cholinergic neurotransmitters in the brain can increase. This helps to protect brain cells by reducing harmful oxidative stress and improving memory and thinking abilities[16].

Cholinesterase inhibitors work by raising ACh concentrations at synapses in the brain and are among the limited drug treatments shown to be effective for managing (AD) dementia. This demonstrates the importance of the cholinergic system as a key target for treatment[11]. Plant extracts have shown therapeutic and preventive effects against Alzheimer's disease (AD) by reducing inflammation and oxidative stress[17,18]. In another study, Apelin is reported to show neuroprotective effects by suppressing inflammation and reduced serum apelin-13 levels in AD highlighting its potential as a therapeutic target[19].

Thiosemicarbazones are a versatile class of compounds known for a wide range of pharmacological activities including antifungal, anticancer[20,21], antiviral antimicrobial, and antiparasitic activities[22,23]. More recently, they have shown promise in treating neurodegenerative disorders due to their ability to inhibit AChE and BChE, thereby enhancing acetylcholine levels and supporting cognitive function[24–26]. At present, a variety of medications are used to treat (AD), such as rivastigmine, donepezil, memantine, galantamine and aducanumab[27–29]. Recent studies have highlighted thiosemicarbazone derivatives as promising multi-target agents for (AD), owing to their inhibitory effects on AChE, BChE and MAOs, along with notable antioxidant and neuroprotective properties Fig. 1.

Heterocyclic derivatives serve as valuable scaffolds for developing potential enzyme inhibitors against Alzheimer's disease (AD)[30,31]. Pharmacophore hybridization has been reported to combines multiple pharmacophoric features into one molecule to improve binding and efficacy[32]. Although thiosemicarbazones and quinoline-based derivatives have been extensively investigated for their biological potential[1,17,33], the introduction of a 4-phenyl-8-quinoline sulfonyl moiety into thiosemicarbazones have not yet been explored. This novel structural modification is anticipated to improve binding infinity, selectivity and biological activity.

Accordingly, the present study reports the synthesis of 4-phenyl-8-quinoline sulfonyl based thiosemicarbazones and evaluates their activity against key Alzheimer's related enzymes[34–36].

Result and discussion

Chemistry

4-Phenyl-quinoline-8-sulfonate based thiosemicarbazones **5(a–r)** were efficiently synthesized as depicted in Fig. 2. The synthesis involved two steps. Initially, 4-formylphenyl quinoline-8-sulfonate **(3)** was obtained by the

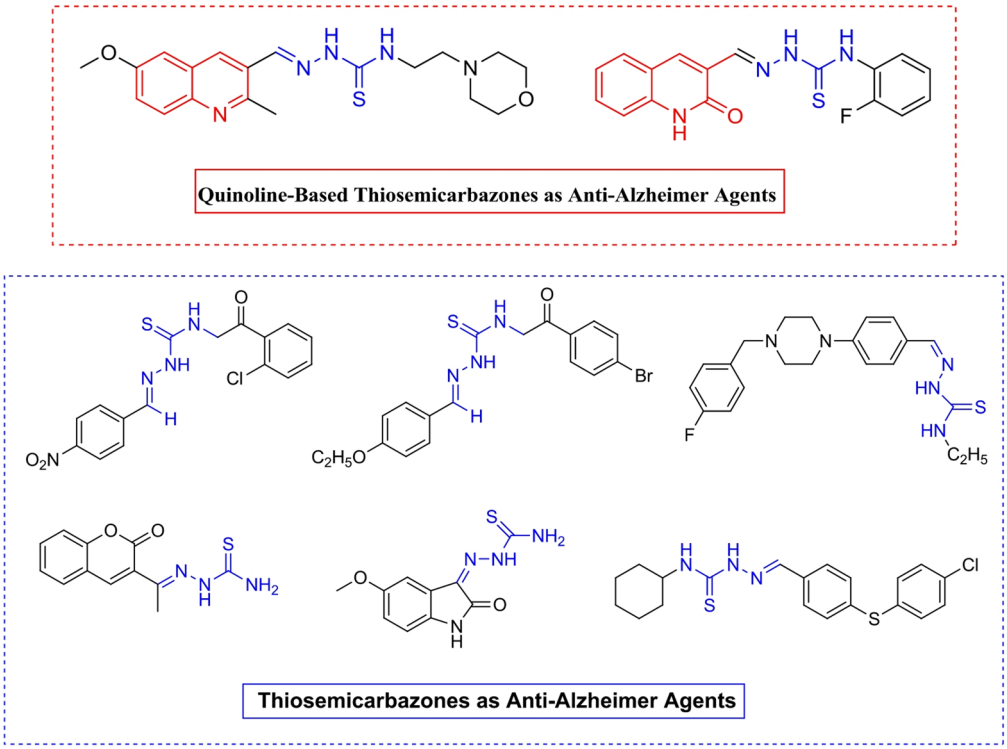

Fig. 1. Reported thiosemicarbazones as potential anti-Alzheimer agents[34–36].

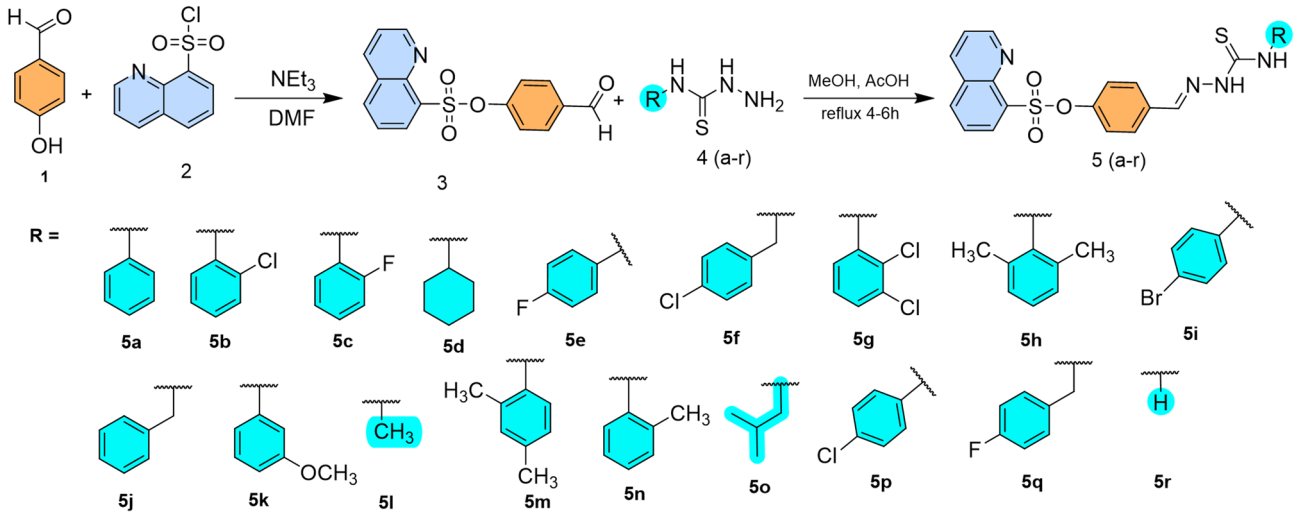

Fig. 2. Synthetic Route of 4-phenyl-quinoline-8-sulfonate based thiosemicarbazones.

reaction of 4-hydroxybenzaldehyde with quinoline-8-sulfonyl chloride in dimethylformamide, in the presence of triethylamine. In the next step, equimolar amounts of compound **3** and the corresponding thiosemicarbazides **4(a–r)** were refluxed in methanol, with acetic acid facilitating the reaction to produce the proposed series of thiosemicarbazone derivatives **5(a–r)**.

The structure of the synthesized thiosemicarbazone derivatives **5(a–r)** was confirmed using ^{1}H and ^{13}C NMR spectroscopy. In the ^{1}H NMR spectra, characteristic signals were observed for the NH–C = S group as singlets within δ 11.43–12.09 ppm, while the NH–N = C moiety resonated in the range of δ 9.23–10.17 ppm. A distinct singlet corresponding to the azomethine proton (HC = N) appeared between δ 7.96–8.08 ppm, indicating successful condensation between the aldehyde and thiosemicarbazide. The ^{13}C NMR data further corroborated the formation of the desired structures.

Biological activity

Structure activity relationship (SAR)

Thiosemicarbazone derivatives **5(a–r)**, derived from the 4-phenyl-quinoline-8-sulfonate scaffold, were evaluated for their inhibitory activity against AChE, BChE and MAO-A using established protocols. The inhibitory effects are depicted in Table 1. The study focus on how R-groups variations in the thiosemicarbazides moiety influence enzyme inhibition. The results demonstrate that R-groups modifications play a crucial role in enhancing bioactivity by influencing enzyme-ligand interactions.

Acetylcholinesterase (AChE) inhibition

In comparison with the reference drug galantamine (IC_{50} = 99.28 µM), several compounds from the 4-phenyl-quinoline-8-sulfonate-based thiosemicarbazone series **5(a–r)** exhibited superior inhibitory effects on acetylcholinesterase, exhibiting IC_{50} values between 75.05 and over 100 µM. The structure–activity relationship was examined by varying the **R** substituent on the thiosemicarbazide framework, and the findings suggest that the nature and position of substituents have a significant influence on the inhibitory potential.

Among the entire series, compound **5 g**, incorporating a 2,3-dichlorophenyl moiety, emerged as the most potent AChE inhibitor, displaying an IC_{50} of 75.05 µM and a K_i of 69.11 µM, indicating a strong affinity for the enzyme. The presence of two electron-withdrawing chlorine atoms at adjacent positions likely enhances binding via improved hydrophobic interactions or a more favorable conformation. This suggests that multiple substitutions, particularly at *ortho*- and *meta*- positions, can significantly enhance inhibitory efficiency.

Similarly, compound **5c** with a 2-fluorophenyl group demonstrated high potency (IC_{50} = 78.07 µM; K_i = 49.33 µM), indicating that *ortho*-substitution with small electronegative atoms like fluorine may support better fitting within the AChE active site. This beneficial effect seems less pronounced when the substituent is at the *para*- position, as seen in **5e** (4-fluorophenyl), which showed slightly lower activity (IC_{50} = 80.15 µM), though still superior to galantamine. Compounds with non-halogen *ortho*- or *para*- substituted phenyl rings, such as **5a** (unsubstituted phenyl), **5n** (2-methylphenyl), and **5o** (sec-butyl), also showed moderate activity with IC_{50} values of 85.36 µM, 86.15 µM, and 81.67 µM, respectively. These findings suggest that a hydrophobic or slightly bulky group can support enzyme binding, but the nature and position of the substituent play a critical role.

In contrast, **5b** (2-chlorophenyl) exhibited an IC_{50} of 92.24 ± 1.62 µM and a K_i of 64.62 ± 6.24 µM, while **5k** (3-methoxyphenyl) showed similar activity with an IC_{50} of 92.09 ± 3.27 µM and a K_i of 89.04 ± 7.33 µM. This noticeable reduction in potency suggests that substitution at the meta position or the presence of bulky polar groups like methoxy may not favor optimal interactions within the AChE active site. Likewise, **5 h** (2,6-dimethylphenyl) recorded an IC_{50} of 92.92 ± 4.04 µM and a K_i of 82.22 ± 7.40 µM, and **5q** (4-fluorobenzyl) displayed an IC_{50} of 93.07 ± 7.68 µM with a K_i of 88.14 ± 11.58 µM. These findings suggest that steric hindrance from multiple *ortho*-substituents (as in **5 h**) or the increased flexibility of benzylic linkers (as in **5q**) likely compromises the compounds' ability to bind efficiently to AChE.

Code	IC_{50} (μM)			Ki (μM)	
	AchE	BChE	MAO-A	AChE	BChE
5a	85.36 ± 2.07	73.20 ± 1.07	5.13 ± 0.07	58.04 ± 4.38	43.76 ± 3.25
5b	92.24 ± 1.62	28.37 ± 0.54	9.22 ± 0.18	64.62 ± 6.24	18.50 ± 1.09
5c	78.07 ± 3.14	22.63 ± 2.81	0.84 ± 0.01	49.33 ± 7.07	12.34 ± 2.84
5d	> 100	56.09 ± 3.22	7.82 ± 0.20	> 100	35.93 ± 4.33
5e	80.15 ± 3.49	34.16 ± 3.07	1.02 ± 0.35	59.07 ± 5.29	19.27 ± 3.06
5f	99.63 ± 4.20	39.42 ± 4.37	6.25 ± 0.01	74.68 ± 8.52	26.03 ± 5.55
5 g	75.05 ± 3.52	24.06 ± 2.52	9.36 ± 0.58	69.11 ± 5.09	20.82 ± 3.20
5 h	92.92 ± 4.04	48.13 ± 4.61	4.07 ± 0.26	82.22 ± 7.40	27.15 ± 2.43
5i	98.44 ± 3.11	53.22 ± 5.07	7.41 ± 0.51	96.37 ± 8.59	31.30 ± 0.76
5j	> 100	57.09 ± 6.41	1.93 ± 0.02	> 100	37.62 ± 4.09
5k	92.09 ± 3.27	62.47 ± 7.22	4.05 ± 0.73	89.04 ± 7.33	40.01 ± 5.26
5 L	> 100	66.15 ± 4.01	6.72 ± 0.15	> 100	33.73 ± 6.48
5 m	> 100	70.92 ± 5.10	11.62 ± 0.29	> 100	48.42 ± 4.31
5n	86.15 ± 3.44	75.57 ± 6.41	17.02 ± 1.81	76.09 ± 8.18	53.19 ± 5.70
5o	81.67 ± 6.28	81.26 ± 4.07	11.47 ± 0.39	70.51 ± 7.22	69.67 ± 3.82
5p	98.41 ± 4.34	56.33 ± 6.13	2.77 ± 0.56	82.29 ± 6.73	44.02 ± 4.53
5q	93.07 ± 7.68	49.52 ± 5.26	1.09 ± 0.09	88.14 ± 11.58	38.33 ± 6.94
5r	> 100	97.01 ± 6.57	17.56 ± 0.33	> 100	72.64 ± 5.07
Galantamine	99.28 ± 3.16	80.27 ± 3.09	–	94.09 ± 7.33	64.06 ± 3.66
Clorgyline	–	–	66.20 ± 4.01	–	–

Table 1. SAR evaluation of compounds **5(a–r)** targeting AChE, BChE, and MAO-A.

Further weakening of activity was observed in **5f** (4-chlorobenzyl, IC_{50} = 99.63 ± 4.20 μM), **5i** (4-bromophenyl, IC_{50} = 98.44 ± 3.11 μM), and **5p** (4-chlorophenyl, IC_{50} = 98.41 ± 4.34 μM). These results suggest that para-halogenation alone, especially in the absence of other supportive substituents or optimal ring orientation, is insufficient to confer strong AChE inhibition. The least active compounds, with IC_{50} values exceeding 100 μM, include **5d** (n-cyclohexyl), **5j** (benzyl), **5 L** (methyl), **5 m** (2,4-dimethylphenyl), and **5r** (hydrogen). These derivatives showed negligible inhibition, suggesting that non-aromatic or overly simple aliphatic groups (as in **5d**, **5 L**, **5r**), or overly bulky substituents (as in **5 m**), result in poor accommodation within the AChE active site. The complete loss of activity in **5r** underscores the importance of having a substantial substituent at the **R** position to support binding interactions.

Butyrylcholinesterase (BChE) inhibition

Among the series, compound **5c** (2-fluorophenyl) exhibited the strongest inhibition of BChE, exhibiting an IC_{50} value of 22.63 μM and K_i of 12.34 μM, indicating a favorable interaction between the fluorine substituent at the *ortho*-position and the enzyme's active site. Likewise, compound **5 g** (2,3-dichlorophenyl) also demonstrated potent inhibition (IC_{50} = 24.06 μM; K_i = 20.82 μM), supporting the beneficial role of multiple electron-withdrawing groups in enhancing binding affinity.

Compound **5b** (2-chlorophenyl) followed closely with an IC_{50} of 28.37 μM, and a relatively low K_i of 18.50 μM, reaffirming the importance of *ortho*-chloro substitution. A similar trend was observed in compound **5e** (4-fluorophenyl), which also showed promising activity (IC_{50} = 34.16 μM; K_i = 19.27 μM), although less effective than its *ortho*-substituted counterparts, suggesting positional sensitivity of halogen atoms.

Moderate BChE inhibition was noted in **5f** (4-chlorobenzyl, IC_{50} = 39.42 μM) and **5 h** (2,6-dimethylphenyl, IC_{50} = 48.13 μM), indicating that either benzylic flexibility or steric hindrance from dual *ortho*-methyl groups may hinder optimal binding. Similarly, **5q** (4-fluorobenzyl) also fell in this mid-range (IC_{50} = 49.52 μM), consistent with the idea that benzylic substitution reduces rigidity and limits interaction strength.

Slightly weaker activity was recorded for **5i** (4-bromophenyl, IC_{50} = 53.22 μM) and **5d** (n-cyclohexyl, IC_{50} = 56.09 μM), suggesting that bulky non-aromatic or heavy halogen groups are less conducive to effective BChE inhibition. Other analogues in this range included **5j** (benzyl, IC_{50} = 57.09 μM) and **5p** (4-chlorophenyl, IC_{50} = 56.33 μM), both showing moderate affinity.

Further reduction in potency was evident in **5k** (3-methoxyphenyl, IC_{50} = 62.47 μM) and **5 L** (methyl, IC_{50} = 66.15 μM), suggesting that small electron-donating groups or lack of aromatic bulk do not sufficiently stabilize the ligand–enzyme complex. This trend continued with **5 m** (2,4-dimethylphenyl, IC_{50} = 70.92 μM) and **5n** (2-methylphenyl, IC_{50} = 75.57 μM), indicating that methylation—particularly at *ortho* or *para* positions—may have limited benefit.

Compound **5o** (sec-butyl) exhibited weak activity (IC_{50} = 81.26 μM), nearly similar to galantamine (IC_{50} = 80.27 μM), highlighting the importance of aromaticity in enhancing inhibition. The least active compound was **5r** (hydrogen), with an IC_{50} of 97.01 μM and K_i of 72.64 μM, reaffirming that the absence of a substituent leads to poor BChE affinity.

Monoamine oxidase-A (MAO-A) inhibition

The evaluation of MAO-A inhibitory activity across the thiosemicarbazone series revealed that several analogues showed remarkable potency, with IC_{50} values significantly lower than the reference inhibitor, clorgyline (IC_{50} = 66.20 µM). The compound **5c** (2-fluorophenyl) displayed the highest potency with an IC_{50} of just 0.84 µM, suggesting that a small electronegative group at the *ortho*-position strongly enhances MAO-A affinity. Similarly, **5e** (4-fluorophenyl) and **5q** (4-fluorobenzyl) also exhibited high potency, with IC_{50} of 1.02 µM and 1.09 µM, respectively. These results indicate that fluorine, whether at the *ortho*- or *para*-position on phenyl or benzyl rings, contributes significantly to enzyme binding, likely via strong electronic effects and favorable positioning within the active site.

Other compounds with excellent activity includes **5j** (benzyl) and **5p** (4-chlorophenyl), with IC_{50} values of 1.93 µM and 2.77 µM, respectively. This suggests that non-substituted benzylic systems and *para*-halogenated aryl rings also support tight binding, possibly due to hydrophobic interactions within the enzyme cavity.

Moderate inhibition was observed for **5 h** (2,6-dimethylphenyl) and **5k** (3-methoxyphenyl), with IC_{50} of 4.07 µM and 4.05 µM, respectively. These results suggest that although steric hindrance from *ortho*- substituents or bulkier polar groups at *meta*- positions can be tolerated, they may reduce optimal binding efficiency.

Compound **5a** (phenyl) displayed moderate inhibition as well (IC_{50} = 5.13 µM), serving as a reference to gauge the effect of substitutions. Introduction of electron-withdrawing groups like chlorine in **5f** (4-chlorobenzyl, IC_{50} = 6.25 µM) or larger hydrophobic substituents in **5d** (n-cyclohexyl, IC_{50} = 7.82 µM) and **5i** (4-bromophenyl, IC_{50} = 7.41 µM) led to reduced potency, possibly due to either steric effects or suboptimal interactions with the active site.

Further reduction in activity was noted in **5b** (2-chlorophenyl, IC_{50} = 9.22 µM) and **5 g** (2,3-dichlorophenyl, IC_{50} = 9.36 µM), where multiple or unfavorably positioned halogens may interfere with proper binding geometry.

Compounds with relatively weak MAO-A inhibition included **5 L** (methyl, IC_{50} = 6.72 µM), **5 m** (2,4-dimethylphenyl, IC_{50} = 11.62 µM), and **5o** (sec-butyl, IC_{50} = 11.47 µM), reflecting that smaller alkyl groups or bulky non-aromatic systems may not contribute positively to binding affinity.

The least effective analogues were **5n** (2-methylphenyl, IC_{50} = 17.02 µM) and **5r** (hydrogen, IC_{50} = 17.56 µM), indicating that minimal or non-functional **R**-groups severely compromise interaction with MAO-A.

The SAR study revealed that electron-withdrawing substituents, particularly ortho-fluorine and *para*-halogen groups, significantly enhance inhibition of AChE, BChE, and MAO-A. Compound **5c** (2-fluorophenyl) consistently showed the highest potency across all three targets, highlighting the critical role of small, electronegative *ortho*-substituents in optimizing enzyme binding affinity Fig. 3.

Molecular docking study

Molecular docking of ache inhibitors

Docking of all active inhibitors of AChE indicates that they bind in the same area of the active site as the co-crystallized inhibitor dihydrotanshinone I Fig. 4. Compounds **5c**, **5e** and **5 g** had were most active AChE inhibitors and had similar activities (IC_{50} = 78.07 ± 3.14, 80.15 ± 3.49 and 75.05 ± 3.52 µM respectively). Hydrogen bonds were found in all three ligands, common amino acids interacting (hydrogen bond) with all three compounds were Ser293, Tyr124, and Tyr341. In addition to these, few unique interactions were also observed for each compound Fig. 5. For compound **5c**, the sulfone group oxygen and NH group were making hydrogen bonds with Arg296 and Ser125 respectively. For compound **5e**, the sulfone group oxygen and NH group were making hydrogen bonds with Ser293 and Ty124 respectively.

For compound **5 g**, the sulfone group oxygen was making a hydrogen bond with Ser293, while the sulfonate oxygen was making a hydrogen with Arg296; its NH groups were making hydrogen bonds with Tyr337. Halogen bonds were also observed for all three compounds with Gly121, Glu202 and Gly120 Table 1S.

The hydrophobic pi-pi T-shaped and pi-pi stacked interactions with Trp86 and the halogen substituted phenyl ring were observed for all three compounds. One of the Cl in **5 g** was additionally making a pi-alkyl interaction with Trp86. pi-Sulfur interactions were observed in **5e** and **5 g** but not in **5c**. The quinoline ring in **5c** and **5e** was

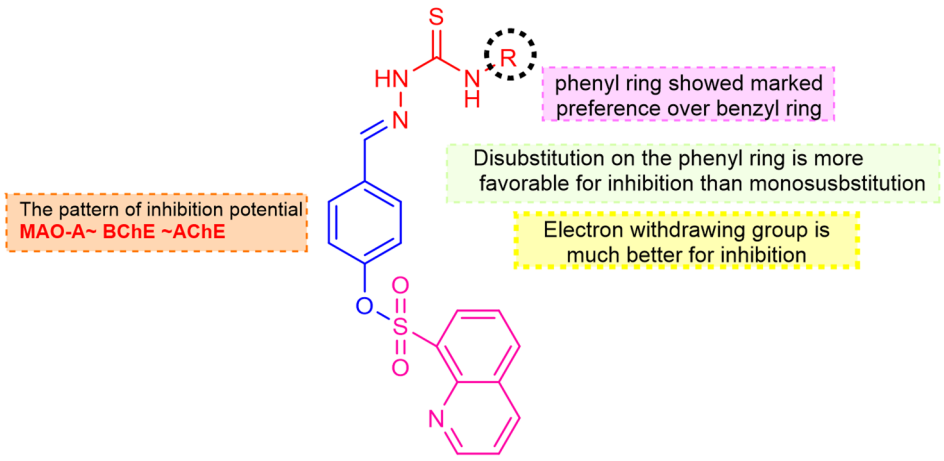

Fig. 3. Illustration of structural diversity and the influence of chemical modifications on biological activity.

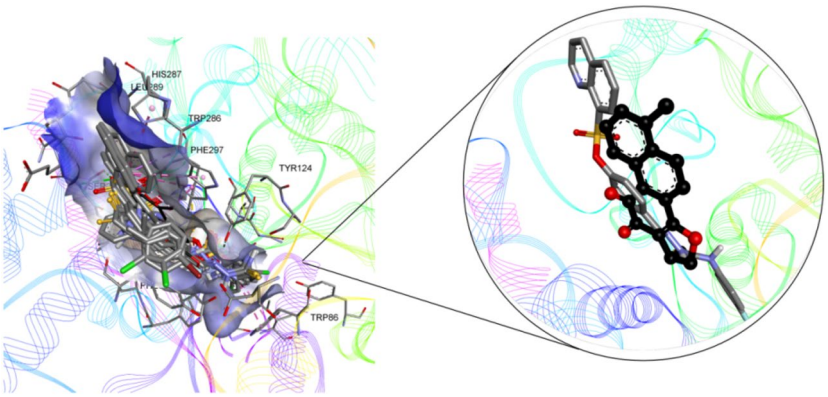

Fig. 4. Overlap of docked conformations of AChE inhibitors with the co-crystallized inhibitor dihydrotanshinone I (represented in black).

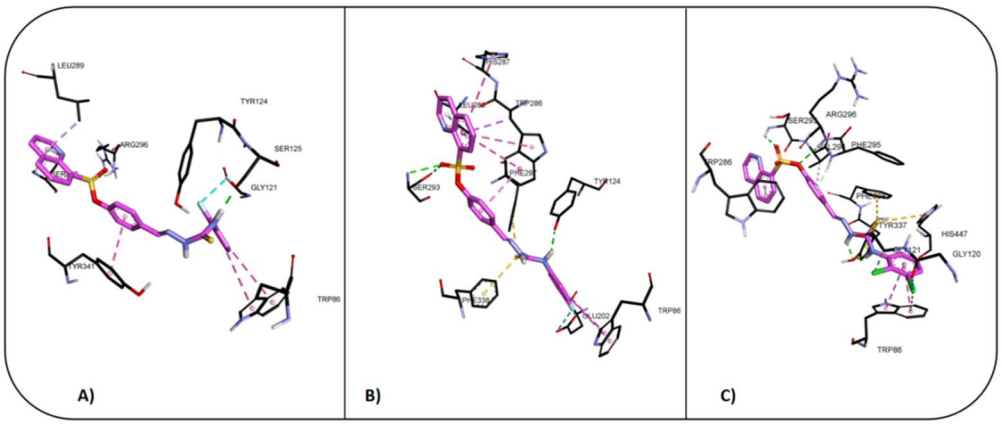

Fig. 5. Binding site interactions of docked conformations of AChE inhibitors (**A**) **5c**, (**B**) **5e** and (**C**) **5 g** indicating similar binding orientation and interactions.

making a pi-sigma and a pi-alkyl interaction with Leu289, while for **5 g** a pi-pi T-shaped interaction with Trp286 was observed. The quinoline ring in **5e** was making pi-pi stacked and a pi-sigma interaction with Trp286, and a pi-pi T-shaped interaction with His287. Compound **5e** showed the strongest pi-pi stacking pattern with Trp286, and halogen bonding with Glu202, not seen in others, hence was selected for MD simulation studies. The phenyl ring in the middle of the molecule was making pi-pi stacked interactions with Tyr341 (in **5c**), Trp286 (in **5e**) and a pi-alkyl with Val294 in **5 g** Fig. 6.

Molecular docking of BChE inhibitors

All compounds were able to inhibit BChE, several compounds exhibited even better inhibition activity than the standard inhibitor. Compounds **5b**, **5c** and **5 g** were most active inhibitors with quite similar IC_{50} values (28.37 ± 0.54, 22.63 ± 2.81 and 24.06 ± 2.52 µM respectively) and were therefore selected for detailed analysis of binding site interactions. Figures 7 and 8 shows overlap of docked conformations of these compounds, showing that they bind in the same area of the binding site as the co-crystallized inhibitor tacrine. Details of these interactions are given in Table 2S.

The oxygen atoms of the sulfone group of **5b**, **5c** and **5 g** were making hydrogen bonds with Gly116, Gly117, and Ala199, indicating interaction with these amino acids is important for enzyme inhibition Fig. 9. Asp70 was involved in hydrogen bonding with the NH groups of compounds **5b** and **5 g**. In compounds **5c** and **5 g** halogen bonds were observed with Pro285 and His438.

The sulfur atom of the sulfone group in all three compounds was found to be making pi-sulfur bonds with aromatic residues His438 and Phe398, while the sulfur atom of the thiocarbonyl group in compounds **5b** and **5 g** was making pi-sulfur bond with Trp430, Tyr332 and Trp82. The quinoline ring in all compounds was making pi-pi T-shaped interactions with Phe329, Trp231, His438 and Trp82. The phenyl ring in the middle of the molecule was making intramolecular pi-pi stacked or pi-pi T-shaped interactions with either the quinoline ring or the other phenyl ring. The terminal phenyl ring in **5c** and **5 g** was making pi-pi stacked interaction with Tyr332, in compound **5 g** a pi-pi T-shaped interaction additionally observed with Phe329. These trends are summarized in Fig. 8.

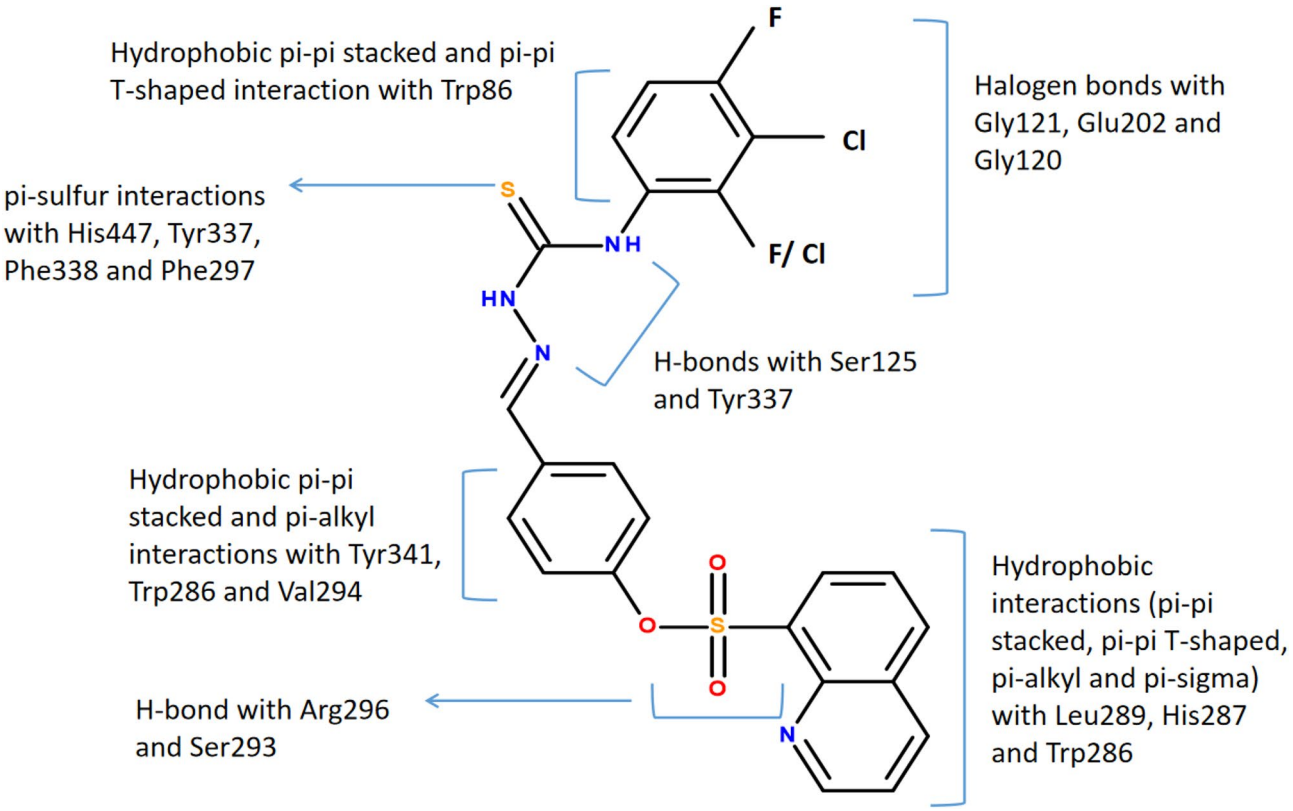

Fig. 6. Summary of binding site interactions of AChE inhibitors **5c**, **5e** and **5 g**.

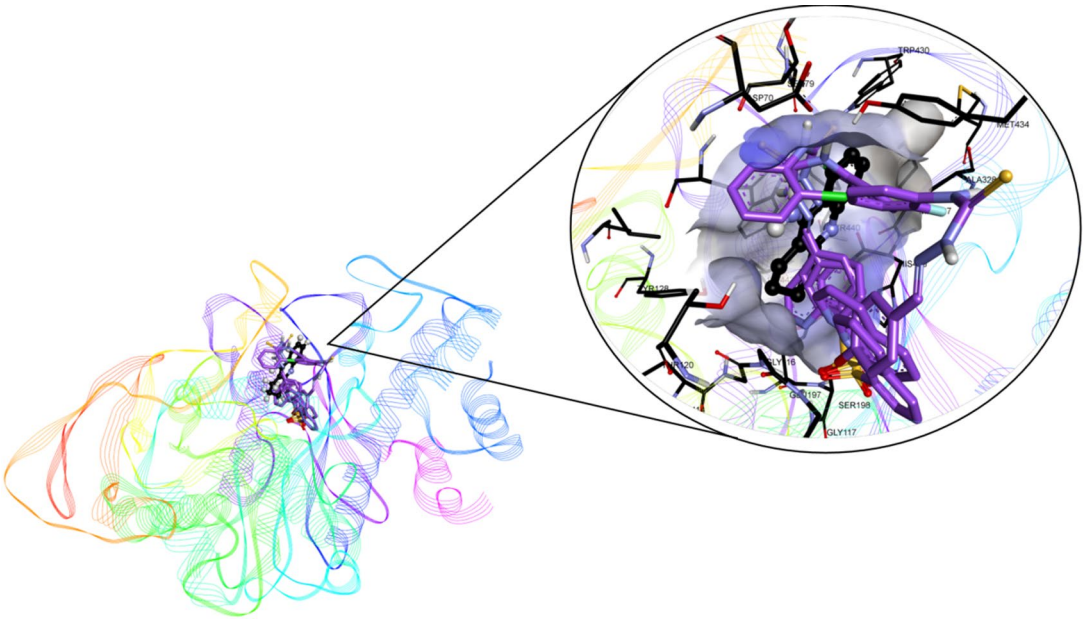

Fig. 7. Overlap of docked conformations of BChE inhibitors **5b**, **5c** and **5 g** with the co-crystallized inhibitor tacrine (represented in black).

Molecular docking studies of MAO A inhibitors

The docking of compounds **5c**, **5e** and **5q** with MAO A showed their orientation near the opening of the active site, covering its entrance Fig. 10, not interacting with the co-factor FAD, unlike the co-crystallized inhibitor harmine. The docking results for **5c**, **5e**, and **5q** revealed both shared and distinct interactions with MAO A. Table 3S shows details of interactions with the binding site residues.

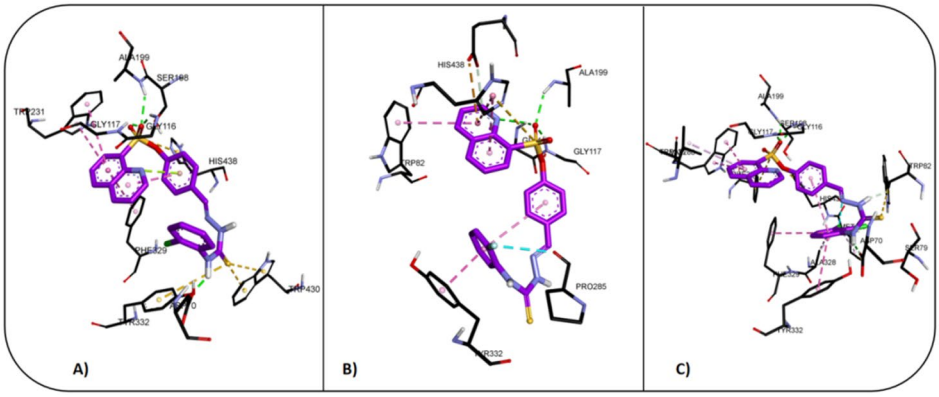

Fig. 8. Binding site interactions of docked conformations of BChE inhibitors (**A**) **5b**, (**B**) **5c** and (**C**) **5 g** indicating similar binding orientation and interactions.

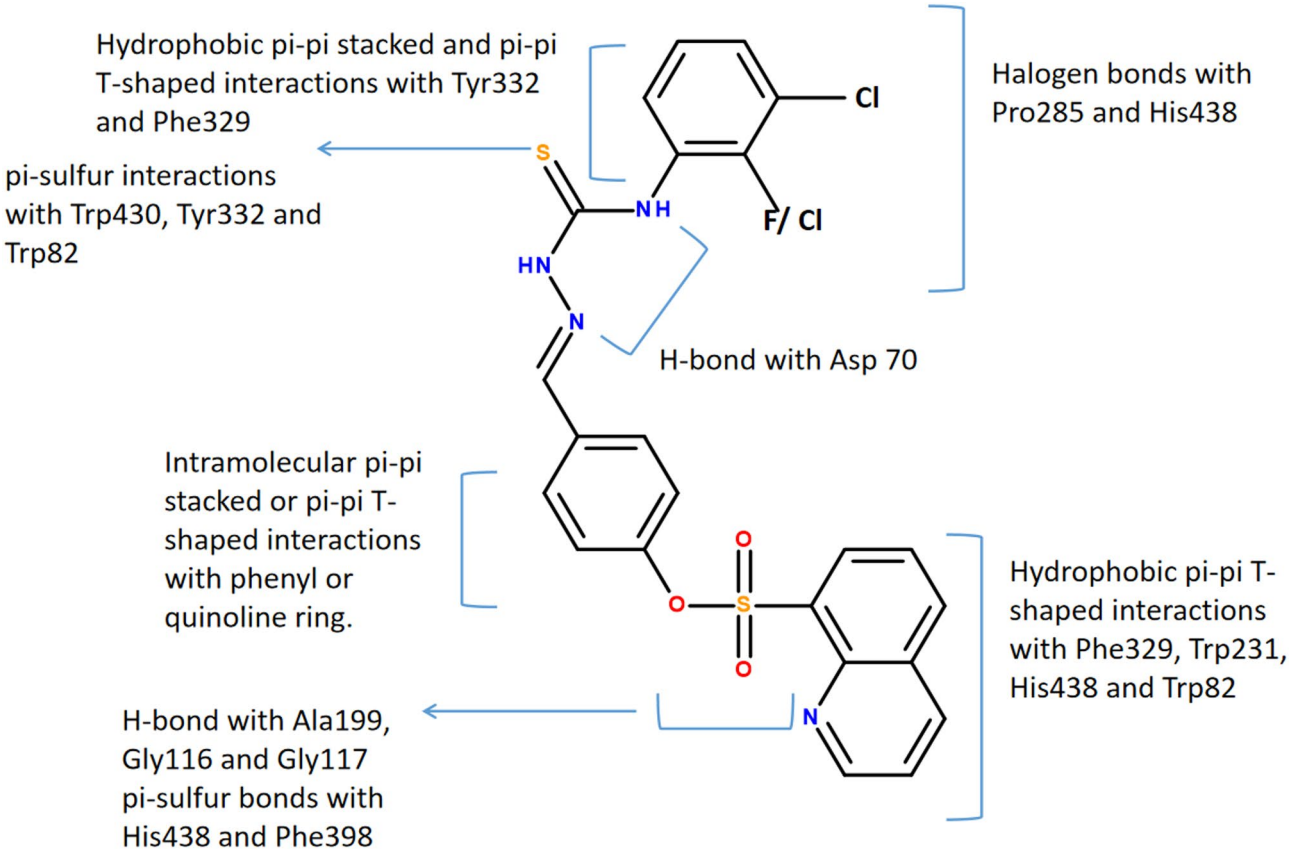

Fig. 9. Summary of binding site interactions of BChE inhibitors **5b**, **5c** and **5 g**.

Ala111 forms hydrogen bonds with the azomethine nitrogen (–C=N–) of **5c** and **5e**, while the NH groups of **5e** and **5q** were making hydrogen bonds with Thr211 and Phe208. The sulfone group oxygen atoms were making hydrogen bonds with Val115 and Gly110. Halogen bonds were observed in **5c** and **5q** with Thr211 and Tyr407. The terminal phenyl ring was making pi-alkyl interactions with Val210, Val93, Ala111 in **5e** and with Leu337 and Ile180 in **5q**. The sulfur atom of the sulfone group was making pi-sulfur interaction with Tyr121 and Tyr124 in **5c** and **5e**. The quinoline ring was making pi-pi T-shaped interactions with Tyr121, Trp116 in 5c and pi-alkyl interaction with Pro114 in **5c** and **5e**, and with Arg109 and Gly110 in **5q** Fig. 11.

The phenyl ring in the middle of the molecule was making pi-donor interaction with Phe112 in **5c** and **5e**; the same ring was also making pi-alkyl interaction with Ala119 in **5c** and **5e**, while for **5q** Val93, Val210, Leu97 and Ala111 were making pi-alkyl interactions with the same phenyl ring Fig. 12. An amide pi stacked interaction was uniquely observed for **5q** between this phenyl ring and Gly110.

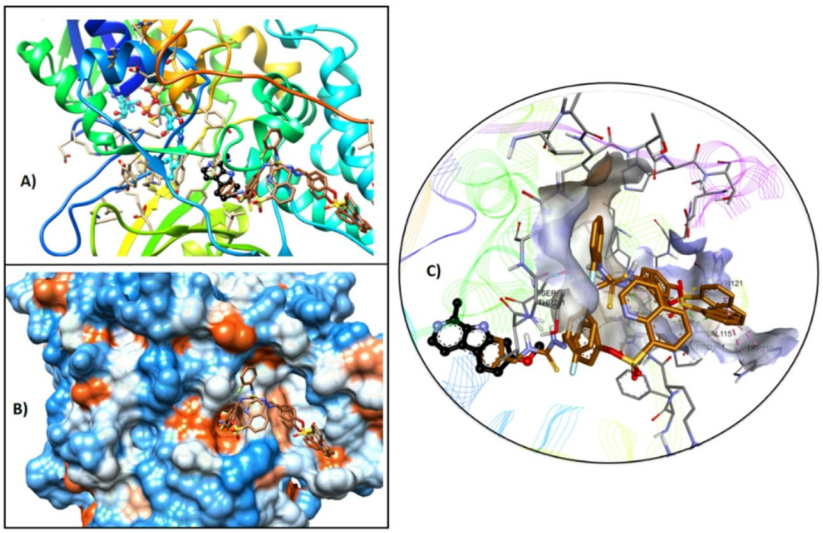

Fig. 10. Overlap of docked conformations of MAO A inhibitors **5c**, **5e** and **5q** with the co-crystallized inhibitor harmine (represented in black) and FAD co-factor (in blue), (**A**) without surface representation, (**B**) with surface representation, (**C**) zoomed-in region showing inhibitors are oriented slightly outward, hindering/covering the opening of the binding site as compared to harmine which is snugged inside the active site.

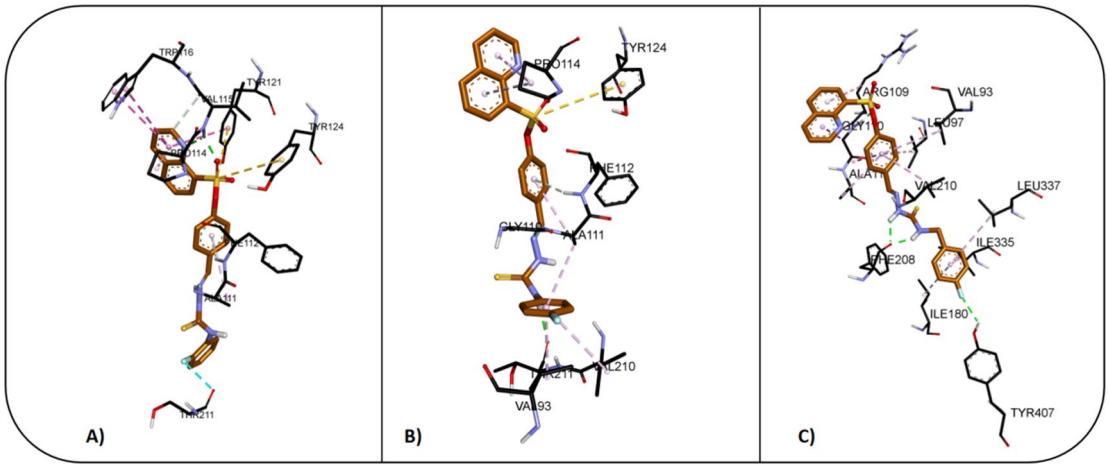

Fig. 11. Binding site interactions of docked conformations of MAO A Inhibitors (**A**) **5c**, (**B**) **5e** and (**C**) **5q**.

Molecular dynamic simulation

Molecular dynamics (MD) simulations are essential tools for exploring the dynamic behaviour, structural flexibility, and stability of protein-ligand complexes at the atomic level, offering critical insights into drug discovery and design. In the present study, 100-nanosecond MD simulations were conducted to evaluate the dynamic stability and interaction patterns of three selected docked complexes: **5e**–AChE, **5 g**–BChE, and 5c–MAO-A. These complexes were chosen based on their favourable docking scores and binding interactions identified during molecular docking studies. The simulations were performed using Desmond software integrated with Schrödinger Maestro 2024.4, under NPT ensemble conditions at 300 K temperature and 1.01325 bar pressure. Each complex was analyzed in terms of root-mean-square deviation (RMSD), root-mean-square fluctuation (RMSF), secondary structure elements (SSE), protein-ligand contacts, and ligand torsion profiles to assess their conformational stability and binding consistency throughout the simulation. The results provided valuable insights into the structural stability and dynamic interaction mechanisms of the selected inhibitors with their respective enzyme targets.

MD simulation studies of ache inhibitor

The MD plot of 5e-AChE complex showed that the C-α RMSD of the protein increased from 1 to 2.4 Å during the first 39ns, after which it stabilized around 2.6 Å for the rest of the simulation. The ligand RMSD (Lig fit on Protein) fluctuated in the range 3.0 Å to 4.8 Å during the simulation and stabilized around 4.2 Å towards

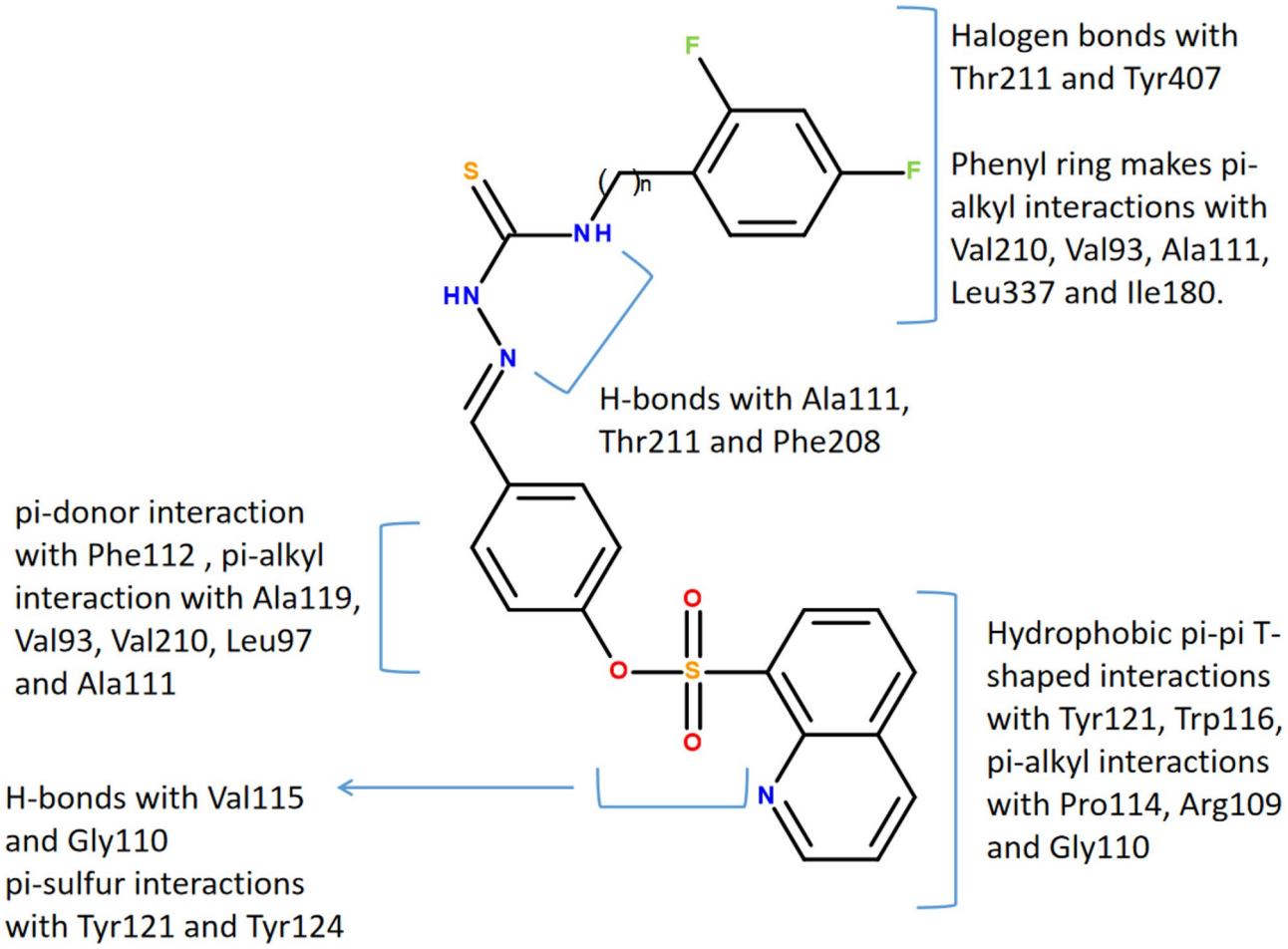

Fig. 12. Summary of binding site interactions of MAO A inhibitors **5c**, **5e** and **5q** (where, $n = 0, 1$).

the end. The internal stability of **5e** (Lig fit on Lig) showed only a slight increase during the initial 20 ns and remained stable between 1.5 Å and 2.0 Å throughout the simulation. The RMSF analysis of the protein showed that most residues showed fluctuations < 3.0 Å, except the C-terminal residues, indicating increased flexibility in this region. The ligand RMSF (Lig fit on Protein) demonstrated that most atoms of **5e** fluctuated around 1.0 Å, with fluorobenzene moiety showing higher flexibility (2.2 Å). Secondary structure analysis (SSE) of the protein showed that 37.67% of the structure was composed of secondary structure elements, including 25.01% α-helices and 12.66% β-strands. Protein-Ligand interaction profile indicated highest interaction fraction by Phe 295 which comprised primarily of hydrogen bonds and water bridges. The sulfonate moiety of **5e** maintained 91% hydrophobic interactions with Phe 295. Phe 338 and Trp 86 maintained 56% and 35% Pi-Pi stacking and hydrophobic interactions with phenyl and fluorobenzene moieties of **5e**, respectively. Tyr 124 showed and maintained 30% hydrophobic interactions with nitrogen of thiosemicarbazone moiety. Torsional analysis showed that all rotatable bonds in **5e** maintained relatively stable torsion angles Fig. 13. The molecular dynamics simulation results of **5e** with AChE showed that the complex remained relatively stable during the whole 100ns simulation time as the protein RMSD value was exhibited below 3.0 Å during the whole simulation. Moreover, RMSD values of **5e**, simulation trajectory, **5e's** ligand RMSF, and torsional profile analysis revealed that **5e** maintained its conformation, orientation, and position of the docked pose with AChE during the whole simulation.

Overall RMSD values suggested that complex attained equilibrium during the simulation Fig. 14.

MD simulation studies of BChE inhibitor

The MD plot of the **5 g**-BChE complex showed that the C-α RMSD fluctuated in the narrow range of 1.25 Å to 2.25 Å during the whole simulation period and remained stabilized around 2.2 Å towards the end. In the **5 g** RMSD graph, the Lig fit on Protein value remained fluctuating between 2.5 Å to 4.5 Å during the simulation and remained around 3.5 Å in the end. **5 g's** Lig fit on lig RMSD value, remained between 1.5 Å to 2.7 Å during the simulation and was around 2.2 Å near the end. The Root-mean-square fluctuation (RMSF) analysis of BChE showed that most residues showed fluctuations < 2.5 Å, except Val 377 (3.14 Å) and the C-terminal residues indicating increased mobility in the loop region. The ligand RMSF profile (Lig fit on Protein) showed that the majority of atoms in compound **5 g** fluctuated below 2.0 Å, suggesting stable binding. However, the indole

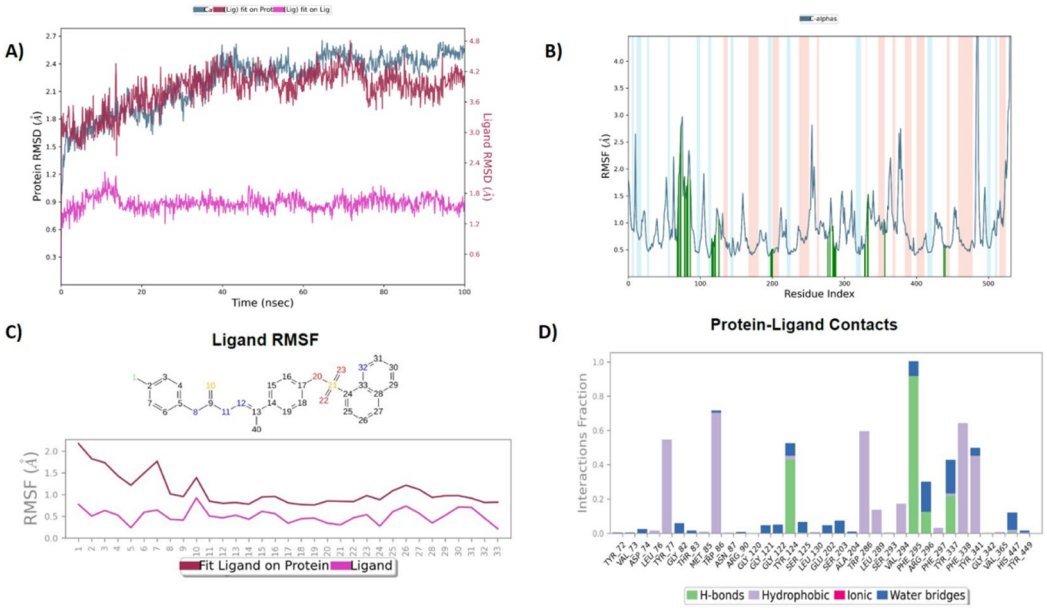

Fig. 13. MD simulation studies of complex of **5e** with AChE for 100ns, (**A**) RMSD plot; (**B**) Protein RMSF graph; (**C**) Ligand RMSF graph and (**D**) protein ligand contacts.

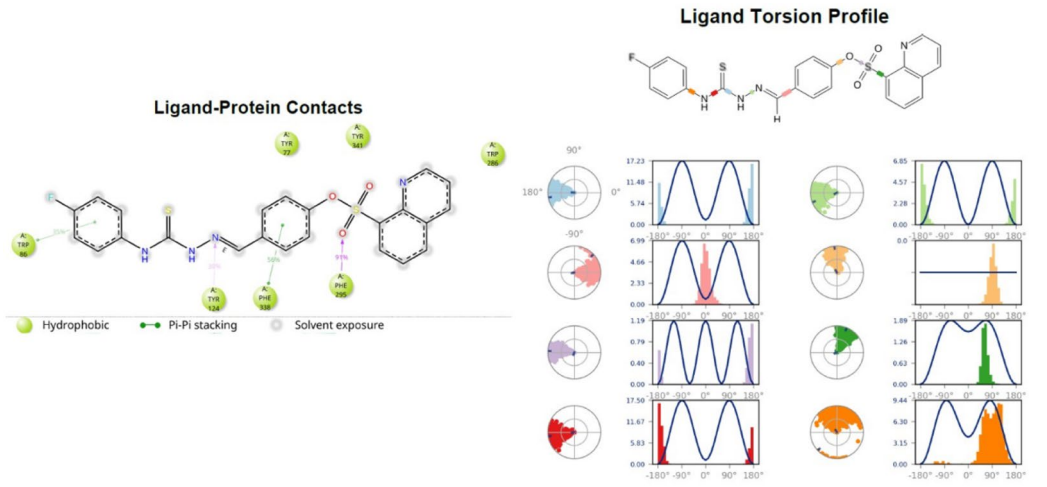

Fig. 14. Ligand Protein Contacts, and Ligand Torsion Profile of **5e** with AChE.

moiety of **5 g** exhibited relatively higher atomic fluctuations, reaching up to 3.5 Å. Secondary Structure analysis of the protein revealed total SSE of 39.39%, comprising of α-helices (25.70%) and β-strands (13.69%). Protein ligand interaction profile revealed that Thr 120 exhibited highest interaction fraction (> 1.0) which consisted primarily of water-bridge-based interactions. Ligand-protein contacts showed that Trp 231 exhibits hydrophobic and Pi-Pi interactions with dichlorobenzene moiety at 43%. While Asn 68 showed polar interactions with indole moiety at 34%. Thr 120 and Gly 116 maintained water-mediated interactions with thiosemicarbazone moiety of 5 g. Torsional analysis demonstrated that all rotatable bonds in compound **5 g** remained conformationally stable throughout the simulation, except for the bond connecting the indole group, which showed slightly increased torsional flexibility Fig. 15.

The molecular dynamics simulation results of **5 g** with BChE showed that the complex remained relatively stable during the whole 100ns simulation time as the protein RMSD value remained below 2.25 Å during the whole simulation. However, RMSD values of **5 g**, simulation trajectory, **5 g** ligand RMSF, and torsional profile analysis revealed that 5 g maintained its docked position, and orientation in the active site of the BChE, however, the dynamic movement was observed in the indole moiety of the compound, which was also corroborated by the trajectory analysis, ligand RMSF, and torsion profile analysis of **5 g**. Overall, **5 g** remained attached to BChE in the active site of the enzyme during the whole simulation period Fig. 16.

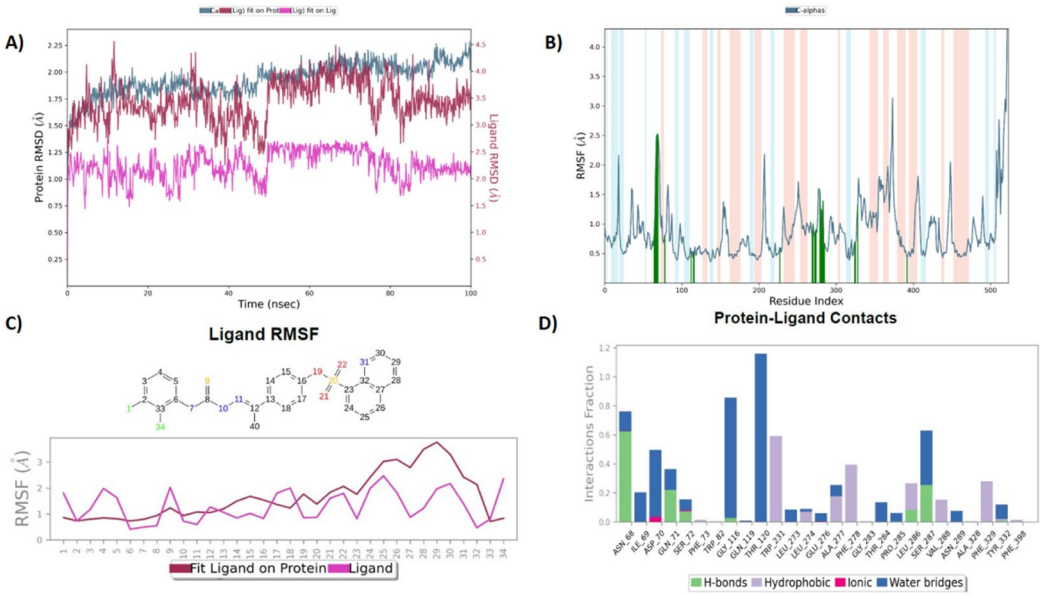

Fig. 15. MD simulation studies of complex of **5 g** with BChE for 100ns, (**A**) RMSD plot; (**B**) Protein RMSF graph; (**C**) Ligand RMSF graph and (**D**) protein ligand contacts.

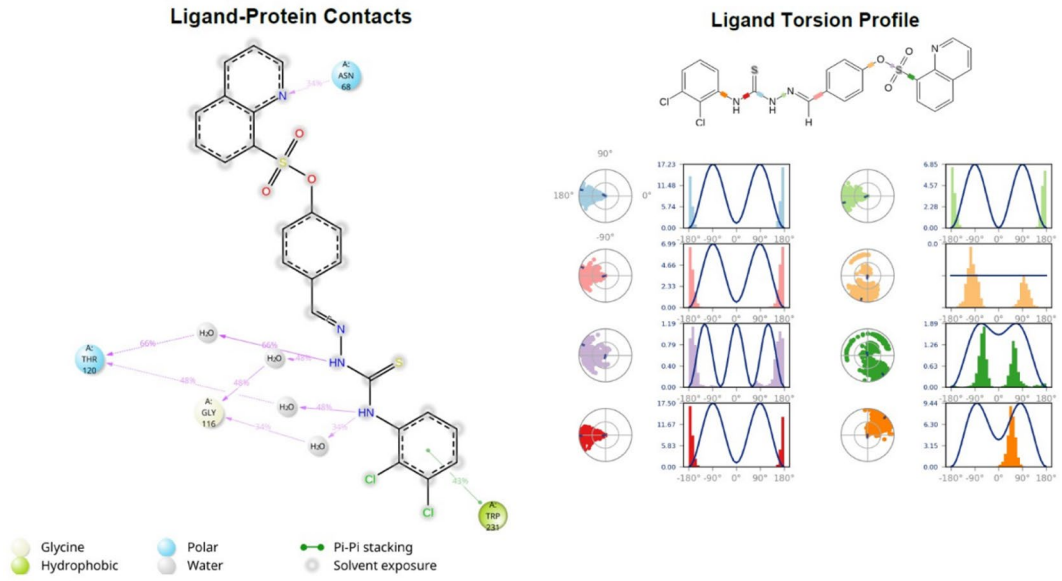

Fig. 16. Ligand Protein Contacts (left), and Ligand Torsion Profile (right) of **5 g** with BChE.

MD simulation studies of MAO A inhibitor

The MD plot of the **5c**-MAO-A complex showed an increase in the C-α Protein RMSD from 1.2 Å to 5.07 Å in the first 13ns, after which the value kept fluctuated around 4.2 Å while raised around 4.8 Å towards the end. The **5c** RMSD graph, showed fluctuation of Lig fit on Protein value between 2.0 Å to 4.5 Å, while remaining around 3.5 Å towards the end of the simulation. A stable ligand RMSD value of approximately 1.75 Å was maintained during most of the simulation. Protein RMSF profile indicated the majority of the protein residues fluctuated less than 2.5 Å, except Asp 343 (2.96 Å), Gly 344 (3.55 Å) and the C-terminal residues. residues involved in binding with ligand 5c demonstrated limited flexibility, with RMSF values under 2.5 Å. Ligand RMSF plot indicated that all ligand (**5c**) atoms fluctuated in a narrow range1.2 Å to 1.75 Å. Secondary Structure analysis of the protein revealed a total SSE content of 42.71%, comprising of α-helices (26.83%) and β-strands (15.88%). Protein-Ligand interaction profile showed that Thr 211 exhibited highest interaction fraction (> 0.8) primarily via water bridges and hydrogen bonds interactions highlighting its key role in ligand stabilization. Ligand-protein contacts reveal that Asn 125 made 70% polar interactions with the sulfonate moiety of **5c**. Trp 128 and Phe 112 maintained

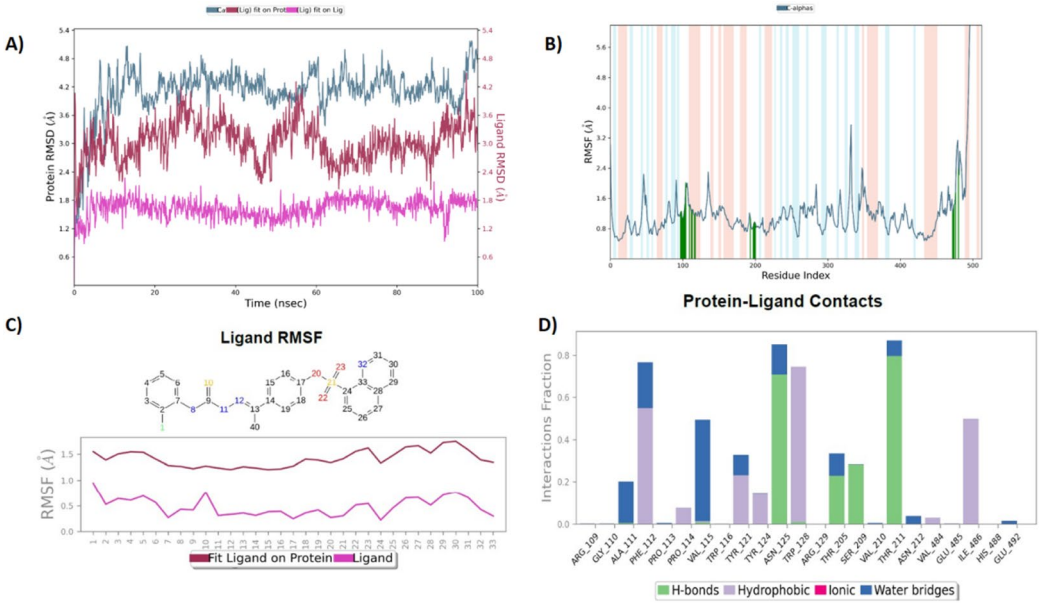

Fig. 17. MD simulation of **5c** with MAO A for 100ns, (**A**) RMSD plot; (**B**) Protein RMSF graph; (**C**) Ligand RMSF graph and (**D**) protein ligand contacts.

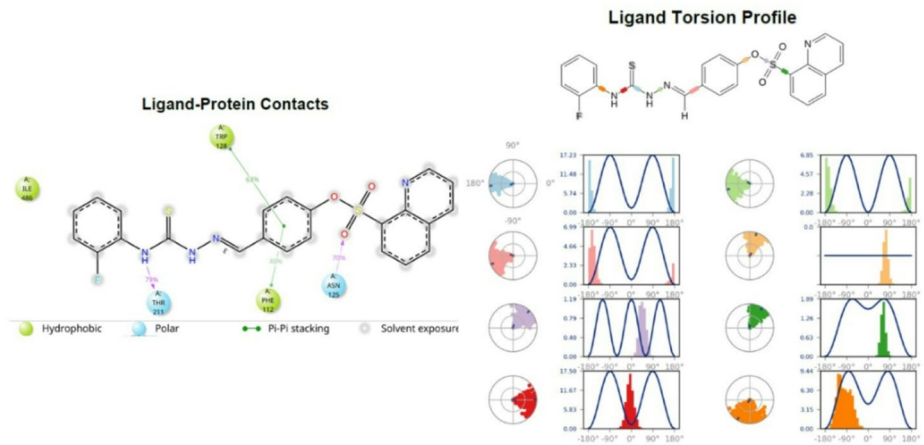

Fig. 18. Ligand Protein Contacts, and Ligand Torsion Profile of **5c** with MAO A.

hydrophobic and π-π stacking interactions with phenyl group at 63% & 45%, respectively. Thr 211 maintained polar interactions at 79% with nitrogen of thiosemicarbazone moiety of **5c**. The torsional profile of compound **5c** indicated minimal fluctuations across all rotatable bonds Fig. 17.

The MD simulation of **5c** with MAO-A revealed that despite RMSD values of protein around 4.8 Å, the complex maintained structural stability throughout the simulation period. Regardless that **5c** is docked at the peripheral site, other than the active site of MAO-A. RMSD values of **5c**, simulation trajectory, Ligand RMSF, and torsional profile analysis revealed that **5c** displayed stable behavior and remained attached with MAO-A in stable docked conformation, position, and orientation during the whole simulation. Moreover, relatively lower RMSF values of MAO-A residues that made contact with **5c** suggest that the interaction of 5c with MAO-A contributed towards the stability of the complex Fig. 18.

Experimental

General

All starting materials, including 4-hydroxybenzaldehyde and triethylamine, were acquired from Sigma-Aldrich and employed directly in the reactions without undergoing additional purification steps. Solvents such as dimethylformamide (DMF), petroleum ether, ethyl acetate, methanol, and acetic acid were purchased from Merck and utilized without modification. Reaction monitoring was carried out through TLC analysis on aluminum-supported silica gel plates.

NMR measurements for both ^{1}H and ^{13}C were carried out at 25 °C using a Bruker Ascend spectrometer, operating at 400 MHz for protons and 101 MHz for carbon nuclei, with DMSO-d_6 as the solvent. All chemical shifts are given in ppm, while coupling constants (*J*) are reported in Hz alongside signal multiplicities. High-resolution mass spectrometry (HRMS) was carried out using electrospray ionization (ESI) on a Thermo Fisher Scientific Q Exactive™ Hybrid Quadrupole-Orbitrap™ instrument. HPLC analyses were performed on a waters e2695 system equipped with Empower 3 software, employing a 1:4 water-acetonitrile mobile phase at a flow rate of 1 mL/min. Peak detection was achieved with PDA detector (model 2998) set at 363 nm.

General procedure for the synthesis of 4-formylphenyl quinoline-8-sulfonate (3)

The synthesis of compound **(3)** was carried out according to previously reported method[24,37]. Briefly, 4-hydroxybenzaldehyde 0.41 g (3.36 mmol) was reacted with 0.477 mL (3.36 mmol) of triethylamine, using 10 mL of dimethylformamide (DMF) as solvent. The mixture was kept in an ice bath with stirring. After 15 min, equimolar amount of quinoline-8-sulfonyl chloride (3.36 mmol) was added dropwise. The reaction mixture was stirred for an additional 1 h, and completion was monitored using thin-layer chromatography (TLC). Upon completion, the mixture was poured into 50 ml of ice-cold water, resulting in the formation of a solid precipitate. The solid was collected by filtration, washed thoroughly with distilled water, and dried to yield the desired product in a good yield.

FTIR (cm^{-1}) 1702 (C = O), 3054 (Ar. C-H). ^{1}H NMR δ_H (400 MHz, Chloroform-*d*) 9.90 (1 H, s), 9.20 (1 H, dd, *J* 4.3, 1.8), 8.40 (1 H, dd, *J* 7.4, 1.5), 8.29 (1 H, dd, *J* 8.4, 1.8), 8.14 (1 H, dd, *J* 8.2, 1.5), 7.83–7.70 (2 H, m), 7.66–7.54 (2 H, m), 7.31–7.19 (2 H, m). ^{13}C NMR (101 MHz, $CDCl_3$) δ 190.66, 154.21, 152.40, 143.90, 136.67, 135.67, 134.64, 134.06, 132.46, 131.18, 129.02, 125.26, 122.84, 122.74.

General procedure for the synthesis of thiosemicarbazones 5(a-r)

A solution of 4-formylphenyl quinoline-8-sulfonate **(3)** (0.1 g, 0.32 mmol) was prepared in 10 mL of methanol with the addition of a catalytic amount of acetic acid (2–3 drops). The mixture was heated under reflux at 70 °C until complete dissolution of the compound. Subsequently, an equimolar amount (0.32 mmol) of the appropriate thiosemicarbazide derivative **4(a–r)** was added to the reaction mixture. Refluxing was continued for 7–8 h, and the reaction progress was monitored periodically by thin-layer chromatography (TLC) until complete consumption of the starting materials.

After completion, the reaction mixture was allowed to cool to room temperature. The resulting solid was collected by filtration, washed thoroughly with methanol to remove impurities, and dried to obtain the final products **5(a-r)**.

(*E*)−4-{[2-(Phenylcarbamothioyl)hydrazono]methyl}phenyl quinoline-8-sulfonate (5a)

Off-white solid. Yield: 63%. Mp: 164–166 °C. FTIR (cm^{-1}) 3217 (N-H), 3054 (Ar. C–H), 1524 (C=N), 1186 (C=S). ^{1}H NMR (400 MHz, DMSO-d_6) δ_H 11.85 (1 H, s), 10.09 (1 H, s), 9.24 (1 H, dd, *J* = 4.3, 1.8 Hz), 8.63 (1 H, dd, *J* = 8.4, 1.8 Hz), 8.46 (1 H, dd, *J* = 8.2, 1.5 Hz), 8.38 (1 H, dd, *J* = 7.4, 1.5 Hz), 8.07 (1 H, s), 7.91–7.71 (4 H, m), 7.53 (2 H, dt, *J* = 8.6, 1.8 Hz), 7.37 (2 H, t, *J* = 7.9 Hz), 7.27–7.15 (1 H, m), 7.07–6.95 (2 H, m). ^{13}C NMR (101 MHz, DMSO-d_6) δ 175.48, 151.87, 149.54, 142.45, 140.51, 138.36, 136.59, 135.81, 133.53, 132.47, 130.62, 128.46, 128.16, 127.44, 125.31, 125.10, 124.78, 122.54, 121.40. ESI-MS: Calculated $[M+H]^+$: 463.089, Found $[M+H]^+$: 463.089; HPLC-PDA: λ 254 nm, MeCN: MeOH (1:1), Rt: 2.89 min, 99.97%.

(*E*)−4-{[2-((2-Chlorophenyl)carbamothioyl)hydrazono]methyl}phenyl quinoline-8-sulfonate (5b)

White solid. Yield: 80%. Mp: 180–182 °C. FTIR (cm^{-1}) 3268, 3152 (N-H), 2984 (Ar. C–H), 1541 (C = N), 1184 (C = S). ^{1}H NMR (400 MHz, DMSO-d_6) δ_H 12.00 (1 H, s), 10.07 (1 H, s), 9.24 (1 H, dd, *J* = 4.2, 1.8 Hz), 8.63 (1 H, dd, *J* = 8.4, 1.8 Hz), 8.46 (1 H, dd, *J* = 8.3, 1.5 Hz), 8.38 (1 H, dd, *J* = 7.4, 1.4 Hz), 8.07 (1 H, s), 7.89–7.70 (4 H, m), 7.62 (1 H, dd, *J* = 7.8, 1.8 Hz), 7.54 (1 H, dd, *J* = 7.9, 1.6 Hz), 7.35 (2 H, dtd, *J* = 25.0, 7.6, 1.7 Hz), 7.09–6.94 (2 H, m). ^{13}C NMR (101 MHz, DMSO-d_6) δ 177.38, 152.95, 150.66, 143.52, 141.68, 137.66, 137.00, 136.89, 134.59, 133.51, 131.71, 131.47, 130.65, 129.77, 129.46, 129.23, 128.44, 127.63, 126.18, 123.61, 122.56. ESI-MS: Calculated $[M+H]^+$: 497.051, Found $[M+H]^+$: 497.050; HPLC-PDA: λ 254 nm, MeCN: MeOH (1:1), Rt: 3 min, 99.97%.

(*E*)−4-{[2-((2-Fluorophenyl)carbamothioyl)hydrazono]methyl}phenyl quinoline-8-sulfonate (5c)

Off-white solid. Yield: 79%. Mp: 116–118 °C. FTIR (cm^{-1}) 3408, 3291, 3106 (N-H), 2955 (Ar. C–H), 1525 (C=N), 1134 (C=S). ^{1}H NMR (400 MHz, DMSO-d_6) δ_H 12.00 (1 H, s), 9.96 (1 H, s), 9.24 (1 H, dd, *J* = 4.2, 1.8 Hz), 8.63 (1 H, dd, *J* = 8.4, 1.8 Hz), 8.46 (1 H, dd, *J* = 8.2, 1.5 Hz), 8.38 (1 H, dd, *J* = 7.4, 1.5 Hz), 8.06 (1 H, s), 7.89–7.70 (4 H, m), 7.47 (1 H, td, *J* = 7.9, 1.8 Hz), 7.27 (3 H, ddtd, *J* = 30.5, 15.1, 7.9, 1.6 Hz), 7.07–6.95 (2 H, m). ^{13}C NMR (101 MHz, DMSO-d_6) δ 177.92, 159.09, 156.63, 152.94, 150.65, 143.52, 141.74, 137.66, 136.89, 134.61, 133.54, 131.69, 130.85, 129.48, 129.23, 128.79, 128.71, 127.58, 127.46, 126.18, 124.50, 124.47, 123.61, 122.50, 116.26, 116.06. ESI-MS: Calculated $[M+H]^+$: 481.080, Found $[M+H]^+$: 481.080; HPLC-PDA: λ 254 nm, MeCN: MeOH (1:1), Rt: 2.87 min, 100%.

(*E*)−4-{[2-(Cyclohexylcarbamothioyl)hydrazono]methyl}phenyl quinoline-8-sulfonate (5d)

White solid. Yield: 71%. Mp: 154–156 °C. FTIR (cm^{-1}) 3356, 3285, 3144 (N–H), 2925 (Ar. C–H), 1521 (C=N), 1139 (C=S). ^{1}H NMR (400 MHz, DMSO-d_6) δ_H 11.43 (1 H, s), 9.25 (1 H, dd, *J* = 4.2, 1.8 Hz), 8.64 (1 H, dd, *J* = 8.4, 1.8 Hz), 8.47 (1 H, dd, *J* = 8.3, 1.5 Hz), 8.37 (1 H, dd, *J* = 7.4, 1.5 Hz), 8.06–7.92 (2 H, m), 7.83 (1 H, dd, *J* = 8.4, 4.2 Hz), 7.79–7.68 (3 H, m), 7.06–6.95 (2 H, m), 4.18 (1 H, dtd, *J* = 11.0, 7.5, 4.2 Hz), 1.84 (2 H, dd, *J* = 12.2, 3.9 Hz), 1.72 (2 H, dt, *J* = 13.1, 3.4 Hz), 1.66–1.54 (1 H, m), 1.39 (2 H, qd, *J* = 12.0, 3.1 Hz), 1.33–1.19 (2 H, m), 1.11 (1 H, ddd, *J* = 15.8, 7.9, 3.4 Hz). ^{13}C NMR (101 MHz, DMSO-d_6) δ 176.18, 152.95, 150.46, 143.51, 140.87, 137.67, 136.89, 134.60, 133.62, 131.67, 129.24, 129.22, 126.17, 123.62, 122.50, 53.17, 32.23, 25.61, 25.42. ESI-MS: Calculated $[M+H]^+$: 469.136, Found $[M+H]^+$: 469.136; HPLC-PDA: λ 254 nm, MeCN: MeOH (1:1), Rt: 3.1 min, 99.98%.

(*E*)−4-{[2-((4-Fluorophenyl)carbamothioyl)hydrazono]methyl}phenyl quinoline-8-sulfonate (5e)

White solid. Yield: 86%. Mp: 218–220 °C. FTIR (cm^{-1}) 3246 (N-H), 3062 (Ar. C–H), 1522 (C=N), 1132 (C=S). ^{1}H NMR (400 MHz, DMSO-d_6) δ_H 11.88 (1 H, s), 10.08 (1 H, s), 9.24 (1 H, dd, J = 4.2, 1.8 Hz), 8.63 (1 H, dd, J = 8.4, 1.8 Hz), 8.46 (1 H, dd, J = 8.2, 1.5 Hz), 8.38 (1 H, dd, J = 7.5, 1.5 Hz), 8.06 (1 H, s), 7.88–7.70 (4 H, m), 7.57–7.44 (2 H, m), 7.25–7.13 (2 H, m), 7.05–6.92 (2 H, m). ^{13}C NMR (101 MHz, DMSO-d_6) δ 175.84, 160.29, 157.88, 151.88, 149.56, 142.45, 140.61, 136.60, 135.83, 134.73, 134.70, 133.54, 132.46, 130.62, 128.46, 128.17, 127.61, 127.53, 125.11, 122.55, 121.40, 114.22, 114.00. ESI-MS: Calculated $[M+H]^+$: 481.080, Found $[M+H]^+$: 481.080; HPLC-PDA: λ 254 nm, MeCN: MeOH (1:1), Rt: 2.87 min, 99.92%.

(*E*)−4-{[2-((4-Chlorobenzyl)carbamothioyl)hydrazono]methyl}phenyl quinoline-8-sulfonate (5f)

Off-white solid. Yield: 95%. Mp: 227–229 °C. FTIR (cm^{-1}) 3279, 3158 (N–H), 2984 (Ar. C–H), 1535 (C=N), 1189 (C=S).^{1}H NMR (400 MHz, DMSO-d_6) δ_H 11.67 (1 H, s), 9.24 (1 H, dd, J = 4.3, 1.8 Hz), 9.11 (1 H, t, J = 6.3 Hz), 8.63 (1 H, dd, J = 8.4, 1.8 Hz), 8.46 (1 H, dd, J = 8.3, 1.5 Hz), 8.37 (1 H, dd, J = 7.4, 1.4 Hz), 8.00 (1 H, s), 7.82 (1 H, dd, J = 8.4, 4.2 Hz), 7.76 (3 H, dd, J = 8.4, 6.1 Hz), 7.46–7.26 (4 H, m), 7.08–6.92 (2 H, m), 4.80 (2 H, d, J = 6.2 Hz). ^{13}C NMR (101 MHz, DMSO-d_6) δ 178.16, 152.93, 150.50, 143.51, 141.07, 138.89, 137.66, 136.88, 134.61, 133.70, 131.70, 131.67, 129.52, 129.22, 129.18, 128.57, 126.16, 123.60, 122.49, 46.36. ESI-MS: Calculated $[M+H]^+$: 511.067, Found $[M+H]^+$: 511.066; HPLC-PDA: λ 254 nm, MeCN: MeOH (1:1), Rt: 3.02 min, 99.92%.

(*E*)−4-{[2-((2,3-Dichlorophenyl)carbamothioyl)hydrazono]methyl}phenyl quinoline-8-sulfonate (5 g)

White solid. Yield: 99%. Mp: 216–218 °C. FTIR (cm^{-1}) 3276, 3151 (N–H), 2980 (Ar. C–H), 1538 (C=N), 1186 (C=S). ^{1}H NMR (400 MHz, DMSO-d_6) δ_H 12.09 (1 H, s), 10.17 (1 H, s), 9.25 (1 H, dd, J = 4.2, 1.8 Hz), 8.63 (1 H, dd, J = 8.4, 1.8 Hz), 8.46 (1 H, dd, J = 8.2, 1.5 Hz), 8.39 (1 H, dd, J = 7.5, 1.5 Hz), 8.08 (1 H, s), 7.88–7.72 (4 H, m), 7.59 (2 H, d, J = 8.0 Hz), 7.46–7.35 (1 H, m), 7.10–6.96 (2 H, m). ^{13}C NMR (101 MHz, DMSO-d_6) δ 177.42, 152.94, 150.71, 143.52, 141.96, 139.15, 137.66, 136.89, 134.59, 133.45, 132.11, 131.70, 130.54, 129.66, 129.50, 129.23, 128.96, 128.10, 126.17, 123.60, 122.56. ESI-MS: Calculated $[M+H]^+$: 531.012, Found $[M+H]^+$: 531.011; HPLC-PDA: λ 254 nm, MeCN: MeOH (1:1), Rt: 3.11 min, 99.61%.

(*E*)−4-{[2-((2,6-Dimethylphenyl)carbamothioyl)hydrazono]methyl}phenyl quinoline-8-sulfonate (5 h)

White solid. Yield: 67%. Mp: 223–225 °C. FTIR (cm^{-1}) 3344, 3113 (N-H), 2966 (Ar. C–H), 1521 (C=N), 1135 (C=S). ^{1}H NMR (400 MHz, DMSO-d_6) δ_H 11.78 (1 H, s), 9.86 (1 H, s), 9.24 (1 H, dd, J = 4.2, 1.8 Hz), 8.63 (1 H, dd, J = 8.4, 1.8 Hz), 8.46 (1 H, dd, J = 8.3, 1.5 Hz), 8.38 (1 H, dd, J = 7.4, 1.5 Hz), 8.04 (1 H, s), 7.91–7.70 (4 H, m), 7.16–7.07 (3 H, m), 7.04–6.92 (2 H, m), 2.16 (6 H, s). ^{13}C NMR (101 MHz, DMSO-d_6) δ 177.31, 152.93, 150.47, 143.53, 140.86, 137.66, 137.52, 136.88, 136.85, 134.60, 133.83, 131.72, 129.40, 129.23, 128.03, 127.37, 126.19, 123.60, 122.43, 18.45. ESI-MS: Calculated $[M+H]^+$: 491.121, Found $[M+H]^+$: 491.121; HPLC-PDA: λ 254 nm, MeCN: MeOH (1:1), Rt: 2.91 min, 99.75%.

(*E*)−4-{[2-((4-Bromophenyl)carbamothioyl)hydrazono]methyl}phenyl quinoline-8-sulfonate (5i)

Off-white solid. Yield: 75%. Mp: 234–235 °C. FTIR (cm^{-1}) 3328, 3115 (N–H), 2973 (Ar. C–H), 1534 (C=N), 1135 (C=S). ^{1}H NMR (400 MHz, DMSO-d_6) δ_H 11.96 (1 H, s), 10.11 (1 H, s), 9.25 (1 H, dd, J = 4.2, 1.8 Hz), 8.72–8.56 (1 H, m), 8.46 (1 H, d, J = 8.2 Hz), 8.45–8.33 (1 H, m), 8.08 (1 H, s), 7.92–7.73 (4 H, m), 7.55 (4 H, s), 7.02 (2 H, d, J = 8.4 Hz). ^{13}C NMR (101 MHz, DMSO-d_6) δ 176.45, 152.94, 150.69, 143.52, 141.97, 138.86, 137.66, 136.89, 134.61, 133.45, 131.69, 131.34, 129.59, 129.23, 128.28, 126.17, 123.61, 122.50, 118.10. ESI-MS: Calculated $[M+H]^+$: 541.000, Found $[M+H]^+$: 541.000; HPLC-PDA: λ 254 nm, MeCN: MeOH (1:1), Rt: 3.04 min, 99.86%.

(*E*)−4-{[2-(Benzylcarbamothioyl)hydrazono]methyl}phenyl quinoline-8-sulfonate (5j)

White solid. Yield: 57%. Mp: 130–132 °C. FTIR (cm^{-1}) 3330, 3116 (N–H), 2958 (Ar. C–H), 1527 (C=N), 1124 (C=S). ^{1}H NMR (400 MHz, DMSO-d_6) δ_H 11.63 (1 H, s), 9.23 (1 H, dd, J = 4.2, 1.8 Hz), 9.08 (1 H, t, J = 6.3 Hz), 8.62 (1 H, dd, J = 8.4, 1.8 Hz), 8.45 (1 H, dd, J = 8.3, 1.5 Hz), 8.36 (1 H, dd, J = 7.5, 1.5 Hz), 7.99 (1 H, s), 7.81 (1 H, dd, J = 8.4, 4.2 Hz), 7.75 (3 H, dd, J = 8.4, 6.5 Hz), 7.37–7.28 (4 H, m), 7.23 (1 H, dq, J = 7.7, 2.8 Hz), 7.03–6.92 (2 H, m), 4.82 (2 H, d, J = 6.2 Hz). ^{13}C NMR (101 MHz, DMSO-d_6) δ 178.12, 152.94, 150.46, 143.51, 140.93, 139.82, 137.66, 136.89, 134.61, 133.73, 131.66, 129.22, 129.17, 128.61, 127.62, 127.17, 126.17, 123.60, 122.49, 47.01. ESI-MS: Calculated $[M+H]^+$: 477.105, Found $[M+H]^+$: 477.105; HPLC-PDA: λ 254 nm, MeCN: MeOH (1:1), Rt: 2.92 min, 99.83%.

(*E*)−4-{[2-((3-Methoxyphenyl)carbamothioyl)hydrazono]methyl}phenyl quinoline-8-sulfonate (5k)

Off-white solid. Yield: 93%. Mp: 177–179 °C. FTIR (cm^{-1}) 3302 (N–H), 2938 (Ar. C–H), 1549 (C=N), 1135 (C=S). ^{1}H NMR (400 MHz, DMSO-d_6) δ_H 11.88 (1 H, s), 10.04 (1 H, s), 9.25 (1 H, dd, J = 4.2, 1.8 Hz), 8.63 (1 H, dd, J = 8.4, 1.8 Hz), 8.46 (1 H, dd, J = 8.3, 1.5 Hz), 8.39 (1 H, dd, J = 7.5, 1.5 Hz), 8.08 (1 H, s), 7.94–7.68 (4 H, m), 7.35–7.23 (2 H, m), 7.23–7.10 (1 H, m), 7.11–6.96 (2 H, m), 6.88–6.72 (1 H, m), 3.77 (3 H, s). ^{13}C NMR (101 MHz, DMSO-d_6) δ 176.28, 159.46, 152.94, 150.65, 143.53, 141.68, 140.53, 137.66, 136.89, 134.60, 133.50, 131.70, 129.57, 129.23, 129.21, 126.17, 123.61, 122.49, 118.32, 111.80, 111.29, 55.62. ESI-MS: Calculated $[M+H]^+$: 493.100, Found $[M+H]^+$: 493.100; HPLC-PDA: λ 254 nm, MeCN: MeOH (1:1), Rt: 2.88 min, 99.89%.

(*E*)−4-{[2-(Methylcarbamothioyl)hydrazono]methyl}phenyl quinoline-8-sulfonate (5 L)

Pale yellow solid. Yield: 58%. Mp: 199–201 °C. FTIR (cm^{-1}) 3358, 3131 (N–H), 2979 (Ar. C–H), 1551 (C=N), 1166 (C=S). ^{1}H NMR (400 MHz, DMSO-d_6) δ_H 11.52 (1 H, s), 9.25 (1 H, dd, J = 4.3, 1.8 Hz), 8.64 (1 H, dd, J = 8.4, 1.8 Hz), 8.55–8.43 (2 H, m), 8.38 (1 H, dd, J = 7.4, 1.5 Hz), 7.96 (1 H, s), 7.83 (1 H, dd, J = 8.4, 4.2 Hz), 7.80–7.69 (3 H, m), 7.06–6.95 (2 H, m), 3.00 (3 H, d, J = 4.6 Hz). ^{13}C NMR (101 MHz, DMSO-d_6) δ 178.23, 152.94, 150.38, 143.52, 140.37, 137.66, 136.87, 134.60, 133.83, 131.70, 129.23, 129.03, 126.17, 123.61, 122.50, 31.26. ESI-MS: Calculated $[M+H]^+$: 401.074, Found $[M+H]^+$: 401.074; HPLC-PDA: λ 254 nm, MeCN: MeOH (1:1), Rt: 2.85 min, 99.91%.

(*E*)−4-{[2-((2,4-Dimethylphenyl)carbamothioyl)hydrazono]methyl}phenyl quinoline-8-sulfonate (5 m)

White solid. Yield: 33%. Mp: 239–241 °C. FTIR (cm^{-1}) 3144 (N–H), 2983 (Ar. C–H), 1532 (C=N), 1137 (C=S). ^{1}H NMR (400 MHz, DMSO-d_6) δ_H 11.76 (1 H, s), 9.87 (1 H, s), 9.23 (1 H, dd, J = 4.2, 1.8 Hz), 8.63 (1 H, dd, J = 8.4, 1.8 Hz), 8.46 (1 H, dd, J = 8.2, 1.5 Hz), 8.37 (1 H, dd, J = 7.4, 1.5 Hz), 8.02 (1 H, s), 7.87–7.70 (4 H, m), 7.12–7.03 (2 H, m), 7.02–6.91 (3 H, m), 2.28 (3 H, s), 2.14 (3 H, s). ^{13}C NMR (101 MHz, DMSO-d_6) δ 177.54, 152.94, 150.49, 143.52, 140.99, 137.67, 136.88, 136.32, 135.89, 135.68, 134.60, 133.75, 131.70, 131.06, 129.40,

129.23, 129.02, 126.92, 126.18, 123.61, 122.45, 21.08, 18.17. ESI-MS: Calculated $[M+H]^+$: 491.121, Found $[M+H]^+$: 491.121; HPLC-PDA: λ 254 nm, MeCN: MeOH (1:1), Rt: 2.95 min, 99.55%.

(*E*)−4-{[2-(*o*-Tolylcarbamothioyl)hydrazono]methyl}phenyl quinoline-8-sulfonate (5n)

Light brown solid. Yield: 67%. Mp: 192–194 °C. FTIR (cm^{-1}) 3336, 3163 (N–H), 2985 (Ar. C–H), 1527 (C=N), 1187 (C=S). ^{1}H NMR (400 MHz, DMSO-d_6) δ_H 11.80 (1 H, s), 9.95 (1 H, s), 9.23 (1 H, dd, J = 4.3, 1.8 Hz), 8.63 (1 H, dd, J = 8.4, 1.8 Hz), 8.46 (1 H, dd, J = 8.3, 1.5 Hz), 8.37 (1 H, dd, J = 7.4, 1.4 Hz), 8.04 (1 H, s), 7.87–7.79 (3 H, m), 7.76 (1 H, dd, J = 8.2, 7.4 Hz), 7.31–7.16 (4 H, m), 7.02–6.92 (2 H, m), 2.19 (3 H, s). ^{13}C NMR (101 MHz, DMSO-d_6) δ 177.41, 152.94, 150.52, 143.52, 141.10, 138.48, 137.67, 136.89, 136.03, 134.60, 133.72, 131.70, 130.51, 129.42, 129.26, 129.23, 127.25, 126.38, 126.19, 123.61, 122.46, 18.23. ESI-MS: Calculated $[M+H]^+$: 477.105, Found $[M+H]^+$: 477.105; HPLC-PDA: λ 254 nm, MeCN: MeOH (1:1), Rt: 2.89 min, 99.96%.

(*E*)−4-{[2-(Sec-butylcarbamothioyl)hydrazono]methyl}phenyl quinoline-8-sulfonate (5o)

Off-white solid. Yield: 66%. Mp: 202–204 °C. FTIR (cm^{-1}) 3353, 3165 (N–H), 2951 (Ar. C–H), 1534 (C=N), 1186 (C=S). ^{1}H NMR (400 MHz, DMSO-d_6) δ_H 11.45 (1 H, s), 9.24 (1 H, dd, J = 4.2, 1.8 Hz), 8.64 (1 H, dd, J = 8.4, 1.8 Hz), 8.53–8.42 (2 H, m), 8.37 (1 H, dd, J = 7.4, 1.4 Hz), 7.96 (1 H, s), 7.82 (1 H, dd, J = 8.4, 4.2 Hz), 7.79–7.70 (3 H, m), 7.05–6.96 (2 H, m), 3.42–3.31 (2 H, m), 2.00 (1 H, dq, J = 13.6, 6.8 Hz), 0.86 (6 H, d, J = 6.8 Hz). ^{13}C NMR (101 MHz, DMSO-d_6) δ 177.74, 152.95, 150.42, 143.52, 140.57, 137.67, 136.89, 134.60, 133.77, 131.69, 129.24, 129.10, 126.18, 123.62, 122.51, 51.26, 28.27, 20.56. ESI-MS: Calculated $[M+H]^+$: 443.121, Found $[M+H]^+$: 443.121; HPLC-PDA: λ 254 nm, MeCN: MeOH (1:1), Rt: 2.98 min, 99.88%.

(*E*)−4-{[2-((4-Chlorophenyl)carbamothioyl)hydrazono]methyl}phenyl quinoline-8-sulfonate (5p)

Off-white solid. Yield: 73%. Mp: 237–239 °C. FTIR (cm^{-1}) 3328, 3127 (N–H), 2978 (Ar. C–H), 1533 (C=N), 1188 (C=S). ^{1}H NMR (400 MHz, DMSO-d_6) δ_H) 11.93 (1 H, s), 10.11 (1 H, s), 9.24 (1 H, dd, J = 4.2, 1.8 Hz), 8.63 (1 H, dd, J = 8.4, 1.8 Hz), 8.46 (1 H, dd, J = 8.3, 1.5 Hz), 8.37 (1 H, dd, J = 7.5, 1.5 Hz), 8.07 (1 H, s), 7.88–7.80 (3 H, m), 7.76 (1 H, t, J = 7.8 Hz), 7.64–7.54 (2 H, m), 7.49–7.37 (2 H, m), 7.07–6.95 (2 H, m). ^{13}C NMR (101 MHz, DMSO-d_6) δ 175.45, 151.88, 149.60, 142.44, 140.85, 137.35, 136.60, 135.82, 133.54, 132.38, 130.61, 128.76, 128.50, 128.16, 127.33, 126.90, 125.10, 122.54, 121.41. ESI-MS: Calculated $[M+H]^+$: 497.051, Found $[M+H]^+$: 497.050; HPLC-PDA: λ 254 nm, MeCN: MeOH (1:1), Rt: 2.99 min, 99.87%.

(*E*)−4-{[2-((4-Fluorobenzyl)carbamothioyl)hydrazono]methyl}phenyl quinoline-8-sulfonate (5q)

White solid. Yield: 87%. Mp: 154–156 °C. FTIR (cm^{-1}) 3331, 3115 (N–H), 2984 (Ar. C–H), 1544 (C=N), 1125 (C=S). ^{1}H NMR (400 MHz, DMSO-d_6) δ_H 11.64 (1 H, s), 9.23 (1 H, dd, J = 4.2, 1.8 Hz), 9.08 (1 H, t, J = 6.3 Hz), 8.63 (1 H, dd, J = 8.4, 1.8 Hz), 8.45 (1 H, dd, J = 8.3, 1.5 Hz), 8.36 (1 H, dd, J = 7.5, 1.5 Hz), 7.99 (1 H, s), 7.81 (1 H, dd, J = 8.4, 4.2 Hz), 7.79–7.70 (3 H, m), 7.43–7.30 (2 H, m), 7.23–7.07 (2 H, m), 7.06–6.94 (2 H, m), 4.79 (2 H, d, J = 6.2 Hz). ^{13}C NMR (101 MHz, DMSO-d_6) δ 178.06, 162.81, 160.40, 152.94, 150.48, 143.51, 141.02, 137.67, 136.89, 136.01, 135.99, 134.61, 133.70, 131.66, 129.69, 129.61, 129.22, 129.17, 126.17, 123.61, 122.49, 115.43, 115.22, 46.29. ESI-MS: Calculated $[M+H]^+$: 495.096, Found $[M+H]^+$: 495.096; HPLC-PDA: λ 254 nm, MeCN: MeOH (1:1), Rt: 2.9 min, 99.90%.

(*E*)−4-[(2-Carbamothioylhydrazono)methyl]phenyl quinoline-8-sulfonate (5r)

White solid. Yield: 91%. Mp: 230–232 °C. FTIR (cm^{-1}) 3379, 3259, 3157 (N–H), 3019 (Ar. C–H), 1562 (C=N), 1190 (C=S). ^{1}H NMR (400 MHz, DMSO-d_6) δ_H 11.47 (1 H, s), 9.25 (1 H, dd, J = 4.2, 1.8 Hz), 8.64 (1 H, dd, J = 8.4, 1.8 Hz), 8.47 (1 H, dd, J = 8.2, 1.4 Hz), 8.38 (1 H, dd, J = 7.5, 1.5 Hz), 8.24 (1 H, s), 8.01 (1 H, s), 7.97 (1 H, s), 7.83 (1 H, dd, J = 8.3, 4.2 Hz), 7.80–7.72 (3 H, m), 7.07–6.95 (2 H, m). ^{13}C NMR (101 MHz, DMSO-d_6) δ 178.54, 152.94, 150.46, 143.51, 140.98, 137.65, 136.87, 134.57, 133.73, 131.71, 129.22, 129.18, 126.16, 123.60, 122.50. ESI-MS: Calculated $[M+H]^+$: 387.058, Found $[M+H]^+$: 387.058; HPLC-PDA: λ 254 nm, MeCN: MeOH (1:1), Rt: 2.76 min, 99.93%.

Inhibition assays

Activity and inhibition test for ache and BChE

Both acetylcholine iodide (AChI) and butyrylcholine iodide (BChI) were employed as substrates for enzymatic hydrolysis reactions, with 5,5′-dithiobis(2-nitrobenzoic acid) (DTNB) used as a chromogenic reagent to detect the activities of AChE and BChE. The assay was carried out as follows: 1 mL of 1.0 M Tris-HCl buffer (pH 8.0) was mixed with 10 µL of the test sample (prepared in deionized water). To this mixture, 50 µL of AChE or BChE enzyme solution was added, and the reaction mixture was incubated at room temperature for 10 min. Following incubation, 50 µL of DTNB solution (0.5 mM) was added, and the enzymatic reaction was initiated by the addition of 50 µL of either AChI or BChI (10 mM). The hydrolysis of the substrates was monitored spectrophotometrically by measuring the absorbance at 412 nm, corresponding to the formation of the yellow-colored 5-thio-2-nitrobenzoate anion. This colorimetric change results from the reaction of DTNB with thiocholine, which is released upon enzymatic hydrolysis of AChI or BChI.

Inhibitory activities were assessed by determining the IC_{50} and K_i values for each compound showing inhibition. For compounds demonstrating inhibitory effects, activity (%)-[I] plots were constructed to calculate the IC_{50} values and the concentrations of inhibitor required to achieve 50% enzyme inhibition. The enzymes used in this study were: BChE from equine serum (C7512) and AChE from *Electrophorus electricus* (electric eel, C3389), both purchased from Sigma-Aldrich[38,39]. We started this investigation with an IC_{50} inhibition analysis. The inhibitor concentration that reduces enzyme activity by half is known as the IC_{50}. Three concentrations were chosen from this paper to start our Ki investigation, and we also examined three distinct inhibitor concentrations using a control. We plotted the Ki graph after determining 1/S and 1/V, then we determined the Ki value according to the graph type (competitive or non-competitive). The Ki's mean and standard deviation were determined and entered into the Table 1.

Study of MAO-A inhibition

The in-vitro fluorometric method was used to evaluate each newly generated substance's inhibitory activity against hMAO-A. In a horseradish peroxidase coupling reaction, the oxired reagent (10-acetyl-3,7-dihydroxyphenoxazine) detects H_2O_2, resulting from the oxidative deamination of tyramine, being utilized as MAO substrate. Firstly, each compound's concentrations of 10^{-3} and 10^{-4} M were studied. In the second step, substances that demonstrated inhibitory activity at a concentration of 10^{-5}–10^{-9} M more than 50% were subjected to additional analysis to find out the IC50 value for hMAO-A isoform as reported in previous studies[24]. The enzymes were purchased from Sigma Aldrich. (M7316-Monoamine Oxidase A human and M7441- Monoamine Oxidase A human)[39].

Computational methods

Molecular docking studies

For molecular docking studies the crystal structures of hMAO (PDB id: 2z5x at 2.20 Å resolution)[40] [, AChE (PDB id: 4m0e at 2.0 Å resolution)[41] and BChE (PDB id: 4bds at 2.10 Å resolution)[42] were downloaded from the PDB. Method validation was ascertained by re-docking the co-crystalized ligand in to the binding site, each time the docking results revealed the docked ligand orientation to be the same as seen in the original crystal structure. For each compound docked, a total of ten docking solutions were generated, each was individually analyzed, finally the one with most favorable binding energy as indicated by the HYDE scoring function of the BioSolveIT's LeadIT (2.3.2, 2017) software (www.biosolveit.de/LeadIT)[43] was selected for detailed analysis of docking interactions. Default docking settings (ligand binding is driven by enthalpy and entropy, hybrid approach) were used. Maximum number of solutions per iteration and maximum number of solutions per fragmentation were also set to default.

Molecular dynamics (MD) simulation studies

Schrödinger Maestro 2024.4 program and Desmond Molecular Dynamics[44] software was utilized for the MD studies of 5c-MAO-A, 5e-AChE, and 5 g-BChE complexes. The best-docked pose complexes of compounds 5c, 5e, and 5 g with MAO-A, AChE, and BChE, respectively, were used as the initial reference structures. In protein preparation, first, the sole respective proteins were processed with the Protein Preparation Wizard of the program for pre-processing and refinement of the structure, then the refined protein structures were complexed with their respective compounds, and subsequently, the complexes were re-run on the protein preparation wizard by keeping all initial parameters the same, except bond order assignment using CCD was kept to missing only for the complexes. The details for the protein preparation and molecular dynamics simulation workflow are mentioned in the supplementary section. An orthorhombic box shape was opted for solvation with pre-defined TIP3P solvent model for water with 10 Å x 10 Å x 10 Å buffer dimensions through the system builder module. Ions placement was done using default values calculated by the software for each respective complex, additionally, to simulate physiological (natural) conditions NaCl (0.15 M) was also included. In the MD simulation was run for 100ns (nanoseconds), trajectory was recorded at every 100ps (picoseconds), resulting in approximately 1000 frames. Default relaxation protocol, NPT ensemble at 1.01325 bar pressure and 300 K temperature using Martyna-Tobias-Klein barostat and Nosé-Hoover chain thermostat settings was used.

Conclusion

A novel series of 4-phenyl-quinoline-8-sulfonate-based thiosemicarbazones **(5a–r)** was synthesized and evaluated for inhibitory activity against AChE, BChE, and MAO-A. The SAR analysis revealed that both the nature and position of aromatic substituents significantly influenced enzyme inhibition. Among the series, compound **5c**, bearing 2-fluorophenyl moiety, exhibited the most potent multi-target activity with IC_{50} values of 78.07 ± 3.14 µM for AChE, 22.63 ± 2.81 µM for BChE, and 0.84 ± 0.01 µM for MAO-A, along with the lowest Ki values across all targets. The enhanced activity of **5c** is attributed to the presence of an *o*-fluoro substituent, likely enhancing binding interactions within the enzyme active sites. Notably, several derivatives demonstrated stronger inhibition of BChE relative to AChE, supporting the therapeutic relevance of BChE inhibition in the advanced stages of (AD). Furthermore, the noticeable MAO-A inhibitory activity was observed, particularly **5c**, which suppressed clorgyline, underscore the dual-target potential of these compounds. The study demonstrates that strategic substitutions significantly influence pharmacological profiles, with compound **5c** emerging as a promising scaffold for designing multifunctional therapeutic targeting key enzymes implicated in (AD).

Data availability

All data generated or analyzed during this study are included in this published article [and its supplementary information files.

Received: 27 July 2025; Accepted: 8 December 2025
Published online: 13 December 2025

References

1. Shrivastava, S. K. et al. Drug reposition-based design, synthesis, and biological evaluation of dual inhibitors of acetylcholinesterase and β-Secretase for treatment of alzheimer's disease. *J. Mol. Struct.* **1262**, 132979 (2022).
2. Rahim, F. et al. Synthesis of new triazole-based thiosemicarbazone derivatives as anti-Alzheimer's disease candidates: Evidence-based in vitro study. *Molecules* **28**, 21 (2022).
3. Tripathi, P. N. et al. Review of pharmacotherapeutic targets in Alzheimer's disease and its management using traditional medicinal plants. *Degener Neurol. Neuromuscul. Disease*. **14**, 47–74 (2024).

4. Anderson, R. M., Hadjichrysanthou, C., Evans, S. & Wong, M. M. Why do so many clinical trials of therapies for alzheimer's disease fail? *Lancet* **390**, 2327–2329 (2017).
5. Scheltens, P. et al. Alzheimer's disease. *Lancet* **388**, 505–517 (2016).
6. Korczyn, A. D. & Grinberg, L. T. Is alzheimer disease a disease? *Nat. Reviews Neurol.* **20**, 245–251 (2024).
7. Sharma, P., Giri, A. & Tripathi, P. N. Emerging trends: Neurofilament biomarkers in precision neurology. *Neurochem. Res.* **49**, 3208–3225 (2024).
8. Selkoe, D. J. & Hardy, J. The amyloid hypothesis of alzheimer's disease at 25 years. *EMBO Mol. Med.* **8**, 595–608 (2016).
9. Wang, J. Z., Xia, Y. Y., Grundke-Iqbal, I. & Iqbal, K. Abnormal hyperphosphorylation of tau: Sites, regulation, and molecular mechanism of neurofibrillary degeneration. *J. Alzheimer's Disease*. **33**, S123–S139 (2012).
10. Scheff, S. W. & Price, D. A. Synaptic pathology in Alzheimer's disease: Aa review of ultrastructural studies. *Neurobiol. Aging*. **24**, 1029–1046 (2003).
11. Hampel, H. et al. The cholinergic system in the pathophysiology and treatment of alzheimer's disease. *Brain* **141**, 1917–1933 (2018).
12. Lane, R. M., Potkin, S. G. & Enz, A. Targeting acetylcholinesterase and butyrylcholinesterase in dementia. *Int. J. Neuropsychopharmacol.* **9**, 101–124 (2006).
13. Tasker, A., Perry, E. K. & Ballard, C. G. Butyrylcholinesterase: Impact on symptoms and progression of cognitive impairment. *Expert Rev. Neurother.* **5**, 101–106 (2005).
14. Naoi, M., Maruyama, W. & Inaba-Hasegawa, K. Type A and B monoamine oxidase in age-related neurodegenerative disorders: Their distinct roles in neuronal death and survival. *Curr. Top. Med. Chem.* **12**, 2177–2188 (2012).
15. Sang, Z., Wang, K., Dong, J. & Tang, L. Alzheimer's disease: Updated multi-targets therapeutics are in clinical and in progress. *Eur. J. Med. Chem.* **238**, 114464 (2022).
16. Jalil, S. et al. Pristine 2-chloroquinoline-based-thiosemicarbazones as multitarget agents against alzheimer's disease: In vitro and in Silico studies of monoamine oxidase (MAO) and cholinesterase (ChE) inhibitors. *J. Mol. Struct.* **1306**, 137841 (2024).
17. Siddiqui, N. et al. Multifaceted neuroprotective role of punicalagin: A review. *Neurochem. Res.* **49**, 1427–1436 (2024).
18. Jia, S., Guan, H., Zhang, S. & Li, Q. Schisandrin A alleviates inflammation and oxidative stress in Aβ25-35-Induced alzheimer's disease in vitro model. *Actas Esp. Psiquiatr.* **52**, 724 (2024).
19. Luo, H. et al. Apelin-13 suppresses neuroinflammation against cognitive deficit in a streptozotocin-induced rat model of alzheimer's disease through activation of BDNF-TrkB signaling pathway. *Front. Pharmacol.* **10**, 395 (2019).
20. Aftab, H. et al. Design, synthesis, in vitro and in Silico studies of novel piperidine derived thiosemicarbazones as inhibitors of dihydrofolate reductase. *Sci. Rep.* **14**, 22645 (2024).
21. Aftab, H. et al. Synthesis, in vitro biological evaluation and in Silico studies of novel pyrrolidine derived thiosemicarbazones as dihydrofolate reductase inhibitors. *RSC Adv.* **14**, 31409–31421 (2024).
22. Bajaj, K., Buchanan, R. M. & Grapperhaus, C. A. Antifungal activity of thiosemicarbazones, Bis (thiosemicarbazones), and their metal complexes. *J. Inorg. Biochem.* **225**, 111620 (2021).
23. Alam, M. et al. Synthesis, characterization, antibacterial activity of thiosemicarbazones derivatives and their computational approaches: Quantum calculation, molecular docking, molecular dynamic, ADMET, QSAR. *Heliyon* **9** (2023).
24. Eshal, J. et al. Synthesis, biological evaluation, and in Silico studies of phenyl naphthalene-2-sulfonate derived thiosemicarbazones as potential carbonic anhydrase inhibitors. *Bioorg. Chem.* **155**, 108118 (2025).
25. Palanimuthu, D. et al. A novel class of thiosemicarbazones show multi-functional activity for the treatment of alzheimer's disease. *Eur. J. Med. Chem.* **139**, 612–632 (2017).
26. Varma, M. et al. Novel alkyl-substituted 4-methoxy benzaldehyde thiosemicarbazones: Multi-target directed ligands for the treatment of alzheimer's disease. *Eur. J. Pharmacol.* **957**, 176028 (2023).
27. Onor, M. L., Trevisiol, M. & Aguglia, E. Rivastigmine in the treatment of alzheimer's disease: An update. *Clin. Interv. Aging*. **2**, 17–32 (2007).
28. Adlimoghaddam, A., Neuendorff, M., Roy, B. & Albensi, B. C. A review of clinical treatment considerations of donepezil in severe alzheimer's disease. *CNS Neurosci. Ther.* **24**, 876–888 (2018).
29. Pardo-Moreno, T. et al. Therapeutic approach to alzheimer's disease: Current treatments and new perspectives. *Pharmaceutics* **14**, 1117 (2022).
30. Gao, X. H., Tang, J. J., Liu, H. R., Liu, L. B. & Liu, Y. Z. Structure–activity study of fluorine or chlorine-substituted cinnamic acid derivatives with tertiary amine side chain in acetylcholinesterase and butyrylcholinesterase Inhibition. *Drug Dev. Res.* **80**, 438–445 (2019).
31. Lu, Q. Q. et al. Nitrogen-containing flavonoid and their analogs with diverse B-ring in acetylcholinesterase and butyrylcholinesterase Inhibition. *Drug Dev. Res.* **81**, 1037–1047 (2020).
32. Kang, L. et al. Structure–activity relationship investigation of coumarin–chalcone hybrids with diverse side-chains as acetylcholinesterase and butyrylcholinesterase inhibitors. *Mol. Diversity*. **22**, 893–906 (2018).
33. Siddiqui, N., Talib, M., Tripathi, P. N., Kumar, A. & Sharma, A. Therapeutic potential of Baicalein against neurodegenerative diseases: An updated review. *Health Sci. Rev.* **11**, 100172 (2024).
34. Basri, R. et al. 2-Oxoquinoline-based-thiosemicarbazones as multitargeting neurotherapeutics against alzheimer's disease: In vitro and in Silico studies of MAO and ChE inhibitors. *Arch. Pharm.* **356**, 2300430 (2023).
35. Uytun, A. N. et al. Synthesis of novel thiosemicarbazone derivatives and investigation of their dual ache and MAO-B inhibitor effects. *J. Mol. Recognit.* **35**, e2990 (2022).
36. Khan, M. et al. Para-substituted thiosemicarbazones as cholinesterase inhibitors: synthesis, in vitro biological evaluation, and in Silico study. *ACS Omega*. **8**, 5116–5123 (2023).
37. Munir, I. et al. Synthesis of 6-ethoxyphenyl 4-fluorobenzenesulfonate-tagged thiosemicarbazones as carbonic anhydrase inhibitors: In-vitro and in Silico approach. *Bioorgan Med. Chem.* **129**, 118301 (2025).
38. Farooq, U. et al. Design, synthesis, in vitro, and in silico studies of 5-(diethylamino)-2-formylphenyl naphthalene-2-sulfonate based thiosemicarbazones as potent anti-Alzheimer agents. *Arch. Pharm.* **358**, e70050 (2025).
39. Ghaffar, U. et al. Synthesis, anti-Alzheimer evaluation and in silico study of 4-mMethoxyphenyl) sulfonyl indole hybrid thiosemicarbazones. *Arch. Pharm.* **358**, e70034 (2025).
40. Son, S. Y. et al. Structure of human monoamine oxidase A at 2.2-Å resolution: The control of opening the entry for substrates/inhibitors. *Proc. Natl. Acad. Sci.* **105**, 5739–5744 (2008).
41. Cheung, J., Gary, E. N., Shiomi, K. & Rosenberry, T. L. Structures of human acetylcholinesterase bound to Dihydrotanshinone I and territrem B show peripheral site flexibility. *ACS Med. Chem. Lett.* **4**, 1091–1096 (2013).
42. Nachon, F. et al. Crystal structures of human cholinesterases in complex with Huprine W and tacrine: Elements of specificity for anti-Alzheimer's drugs targeting acetyl-and butyryl-cholinesterase. *Biochem. J.* **453**, 393–399 (2013).
43. BioSolveIT's LeadIT. 2.3.2, (2017). www.biosolveit.de/LeadIT
44. Desmond, M. D. *System, version 2023.4, D. E* (Shaw Research,).

Acknowledgements

Z.S. is thankful to the ORIC, BZ University, Multan, Pakistan.

Author contributions

R.S., H. Z.T., H.A. and A. A. designed, synthesized and characterized the compounds; N.S. and P.T.K. performed the enzyme inhibition assay; M.a-R, T.I. and H.K.T. performed molecular modeling studies; J.L. provided access to instrumentation; H.S. and M.A. performed FTIR, HRMS, NMR, made graphs and wrote spectra discussion; Z.S. supervised the work and wrote the manuscript with the help of R.S. All authors read and approved the manuscript.

Funding

Z.S. is thankful to the ORIC, BZ University, Multan, Pakistan.

Declarations

Competing interests

The authors declare no competing interests.

Additional information

Supplementary Information The online version contains supplementary material available at https://doi.org/10.1038/s41598-025-32012-y.

Correspondence and requests for materials should be addressed to Z.S.

Reprints and permissions information is available at www.nature.com/reprints.

Publisher's note Springer Nature remains neutral with regard to jurisdictional claims in published maps and institutional affiliations.